

Fast Multitask Gaussian Process Regression

Aleksei G. Sorokin^{a,b,c}, Pieterjan Robbe^b, Fred J. Hickernell^a

^a*Department of Applied Mathematics, Illinois Institute of Technology, 10 W 35th Street, Chicago, 60616, IL, USA*

^b*Sandia National Laboratories, 7011 E Ave, Livermore, 94550, CA, USA*

^c*Department of Statistics, University of Chicago, 5801 S Ellis Ave, Chicago, 60637, IL, USA*

Abstract

Gaussian process (GP) regression is a powerful probabilistic modeling technique with built-in uncertainty quantification. When one has access to multiple correlated simulations (tasks), it is common to fit a multitask GP (MTGP) surrogate which is capable of capturing both inter-task and intra-task correlations. However, with a total of N evaluations across all tasks, fitting an MTGP is often infeasible due to the $\mathcal{O}(N^2)$ storage and $\mathcal{O}(N^3)$ computations required to store, solve a linear system in, and compute the determinant of the $N \times N$ Gram matrix of pairwise kernel evaluations. In the single-task setting, one may reduce the required storage to $\mathcal{O}(N)$ and computations to $\mathcal{O}(N \log N)$ by fitting “fast GPs” which pair low-discrepancy design points from quasi-Monte Carlo to special kernel forms which yields nicely structured Gram matrices, e.g., circulant matrices. This article generalizes fast GPs to fast MTGPs which pair low-discrepancy design points for each task to special product kernel forms which yields nicely structured block Gram matrices, e.g., circulant block matrices. An algorithm is presented to efficiently store, invert, and compute the determinant of such Gram matrices with optionally different sampling nodes and different sample sizes for each task. Derivations for fast MTGP Bayesian cubature are also provided. A GPU-compatible, open-source Python implementation is made available in the FastGPs package (<https://alegresor.github.io/fastgps/>). We validate the efficiency of our algorithm and implementation compared to standard techniques on a range of problems with low numbers of tasks and large sample sizes.

Keywords: fast multitask Gaussian processes, low-discrepancy sequences, quasi-Monte Carlo, multitask Bayesian cubature, structured kernel interpolation

1. Introduction

A common scientific problem is to build a surrogate which simultaneously exploits information from multiple correlated simulations. Such simulations, or tasks, often arise in multifidelity modeling where the different tasks evaluate a simulation at different fidelity levels. The goal is to exploit the cheaper low-fidelity surrogates to accelerate modeling for the more expensive

Email addresses: agsorokin3@gmail.com (Aleksei G. Sorokin), pmrobbe@sandia.gov (Pieterjan Robbe), hickernell@iit.edu (Fred J. Hickernell)

high-fidelity simulation. A common example is numerical PDE solvers where the fidelity setting typically controls the mesh discretization with higher fidelities corresponding to finer meshes and more accurate approximations at greater expense.

Gaussian process (GP) regression (Rasmussen and Williams, 2006) is a powerful probabilistic surrogate modeling technique with built-in uncertainty quantification. GPs have a natural extension to multitask GPs (MTGPs) (Bonilla et al., 2007) which are capable of capturing both inter-task and intra-task correlations. However, for N total points across all simulations, fitting a MTGP requires $\mathcal{O}(N^2)$ storage and $\mathcal{O}(N^3)$ computations in order to store, solve a linear system in, and compute the determinant of the $N \times N$ Gram matrix $\tilde{\mathbf{K}}$ of kernel evaluations at all pairs of design points. These lofty requirements often preclude the use of MTGPs for large scale applications such as those in multifidelity settings where it is common for the cheaper low-fidelity surrogates to permit tens or even hundreds of thousands of evaluations.

Perhaps the most popular technique to reduce the high cost of GP/MTGP fitting is to use a preconditioned conjugate gradient (PCG) method to solve the linear system in the Gram matrix $\tilde{\mathbf{K}}$. As PCG only requires multiplications of $\tilde{\mathbf{K}}$, packages such as GPyTorch (Gardner et al., 2018a) utilize efficient black-box matrix multiplication routines for efficient GPU scaling. For fitting GP hyperparameters (Fasshauer, 2007; Craven and Wahba, 1978; Golub et al., 1979; Wahba, 1990), PCG is often paired with an approximation for the determinant and its gradient using the Lanczos tridiagonalization algorithm and stochastic trace estimation respectively. While PCG-GPs still require $\mathcal{O}(N^2)$ storage, lazy evaluation of $\tilde{\mathbf{K}}$, such as the GPU compatible implementation in the KeOps package (Charlier et al., 2021), may also be used to trade off storage requirements for additional compute.

For well-conditioned $\tilde{\mathbf{K}}$, the number of PCG steps is $\mathcal{O}(1)$, which enables PCG-GP fitting with only $\mathcal{O}(N^2)$ computations. However, in the MTGP setting, one often encounters ill-conditioned $\tilde{\mathbf{K}}$ due to the highly correlated evaluations between tasks. In such cases, the required number of PCG steps is $\mathcal{O}(N)$, bringing the total computational requirement back to the usual $\mathcal{O}(N^3)$.

Another option to overcome the prohibitive storage and computation requirements for GP fitting is to induce structure into $\tilde{\mathbf{K}}$. In the single-task GP setting, one popular technique is to pair d -dimensional regular grids with product kernels which yields Kronecker product $\tilde{\mathbf{K}}$ for which fitting requires only $\mathcal{O}(dn^{2/d})$ storage and $\mathcal{O}(dn^{3/d})$ computations (Saatçi, 2012; Gardner et al., 2018b; Wilson and Nickisch, 2015; Wilson, 2014). If the kernel is also stationary, then $\tilde{\mathbf{K}}$ becomes Toeplitz and the computational requirement can be further reduced to $\mathcal{O}(dn^{1+1/d})$. However, such structured kernel interpolation (SKI) techniques require regular grid sampling nodes that do not scale well to high-dimensions and do not admit diverse marginal projections, although approximate GP schemes do exist for partial grid structures (Wilson et al., 2014). Moreover, even in the low-dimensional setting, it is non-trivial to generalize these structures to the MTGP setting with differing numbers of points for each task. We will explore an adjacent set of SKI methods which scale nearly independently of the dimension d , and we will derive the requisite generalizations to enable fast MTGP fitting with differing sample sizes and sampling locations for each task.

The fast MTGP SKI methods we develop are motivated by single-task “fast GP” methods which pair low-discrepancy (LD) sequences typically used for quasi-Monte Carlo with certain (digitally-)shift-invariant kernels to induce nice structure in $\tilde{\mathbf{K}}$ (Zeng et al., 2009, 2006). In the single-task setting, there are at least two fast GP flavors:

1. Pairing an LD shifted rank-1 lattice sequence with a shift-invariant kernel produces a circulant $\tilde{\mathbf{K}}$ whose eigenvectors correspond to the fast Fourier transform (FFT) (Cooley and Tukey, 1965).
2. Pairing an LD digitally-shifted base-2 digital sequence with a digitally-shift-invariant kernel produces $\tilde{\mathbf{K}}$ whose eigenvectors correspond to the fast Walsh–Hadamard transform (FWHT) (Fino and Algazi, 1976).

These structures in $\tilde{\mathbf{K}}$ enable fast GP fitting with only $O(N)$ storage and $O(N \log N)$ computations. Figure 1 contrasts independent and identically distributed (IID) points against the more even coverage of LD lattices and digital sequences which have historically been used for quasi-Monte Carlo methods (Dick and Pillichshammer, 2010; Dick et al., 2022). These single-task fast GP methods have proven valuable for Bayesian cubature (Rathinavel, 2019; Rathinavel and Hickernell, 2022, 2019; Sorokin et al., 2025a) and solving PDEs with random coefficients (Kaarnioja et al., 2022, 2023; Sorokin et al., 2024). More recently, authors of this article have explored incorporating derivative information into fast GPs with equal sample sizes per task (per derivative) (Sorokin et al., 2025b; Sorokin, 2025a). We generalize the structures explored there to unequal sample sizes per task, and connect derivative informed GPs to a special case of MTGPs, see Remark 2.1 and Remark 2.2.

This article proposes fast MTGPs which pair LD sequences for each task with kernels that may be written as the product of a task kernel and a spatial kernel which we require to be (digitally-)shift-invariant. Specifically, we generalize the enumerated items above to the fast MTGP setting which admits the following two flavors.

1. Pairings shifted rank-1 lattice sequences for each task with a spatially shift-invariant kernel yields $\tilde{\mathbf{K}}$ which is a block matrix with circulant blocks, each of which has eigenvectors corresponding to the FFT.
2. Pairing digitally-shifted base-2 digital sequences for each task with a spatially digitally-shift-invariant kernel yields $\tilde{\mathbf{K}}$ which is a block matrix with each block having eigenvectors corresponding to the FWHT.

Importantly, we allow the LD sequences for each task to have different shifts / digital-shifts, and we allow different sample sizes for each task. This means that the block matrix $\tilde{\mathbf{K}}$ has blocks of different sizes. For fast MTGPs, we factor out the fast transforms eigenvectors from $\tilde{\mathbf{K}}$ and are then left to invert and compute the determinant of a sparse block matrix where each block is diagonal. These operations are efficiently executed using recursive 2×2 block matrix inversion and determinant formulas with the key observation being that, after reindexing tasks, the Schur complements become diagonal. Interestingly, both the required storage and computations for fast MTGPs contain a term $O(N^2/n_L)$ where N is the total number of points and n_L is the number of samples for the task with the least number of points. This implies that our fast MTGPs fitting becomes more efficient when raising the minimum number of samples across tasks.

The novel contributions in this paper are to:

1. Propose an algorithm for efficiently storing, inverting, and computing the determinant of multitask kernel Gram matrices which arise when pairing potentially differing numbers of lattice or digital low-discrepancy sampling sequences for each task with kernels which are

the product of a task kernel and shift-invariant or digitally-shift-invariant spatial kernel respectively.

2. Analyze the storage and computation requirements of the proposed algorithm.
3. Apply this algorithm to fast multitask Gaussian process (MTGP) regression and fast multitask Bayesian cubature.
4. Implement our methods into the GPU-compatible open-source Python package FastGPs (<https://alegresor.github.io/fastgps/>).
5. Validate our fast MTGP regression and cubature routines on a number of problems including multifidelity PDE modeling.

The remainder of this article is organized as follows. [Section 2](#) details standard single-task GPs ([Section 2.1](#)), then fast single-task GPs ([Section 2.2](#)), then standard MTGPs ([Section 2.3](#)), then fast MTGPs ([Section 2.4](#)). [Section 3](#) details our numerical experiments comparing fast MTGPs against standard MTGPs for problems with a few tasks and many evaluations per task. [Section 4](#) provides a brief conclusion.

2. Methods

2.1. Gaussian Processes

Let us begin by defining symmetric positive definite (SPD) kernels on a domain $\mathcal{X} \subseteq \mathbb{R}^d$. Going forward, when we call a function a kernel, it is assumed to be SPD. Our fast GP methods will require $\mathcal{X} = [0, 1]^d$.

Definition 2.1 (Symmetric positive definite kernel). *A function $K : \mathcal{X} \times \mathcal{X} \rightarrow \mathbb{R}$ is SPD kernel on \mathcal{X} if $K(\mathbf{x}, \mathbf{x}') = K(\mathbf{x}', \mathbf{x})$ for any $\mathbf{x}, \mathbf{x}' \in \mathcal{X}$, and $\sum_{i,i'=0}^{n-1} c_i c_{i'} K(\mathbf{x}_i, \mathbf{x}_{i'}) > 0$ for any $n \in \mathbb{N}$, any $c_0, \dots, c_{n-1} \in \mathbb{R}$, and any $\mathbf{x}_0, \dots, \mathbf{x}_{n-1} \in \mathcal{X}$.*

Let us assume $f : \mathcal{X} \rightarrow \mathbb{R}$ is a GP on \mathcal{X} with constant prior mean $\tau \in \mathbb{R}$ and a covariance kernel $K : \mathcal{X} \times \mathcal{X} \rightarrow \mathbb{R}$. We will denote this by $f \sim \text{GP}(\mathbb{E}[f], \text{Cov}[f, f])$ where the prior mean is $\mathbb{E}[f(\mathbf{x})] = \tau$ and the prior covariance is $\text{Cov}[f(\mathbf{x}), f(\mathbf{x}')] = K(\mathbf{x}, \mathbf{x}')$ for any $\mathbf{x}, \mathbf{x}' \in \mathcal{X}$.

Perhaps the most popular choice of K is the squared exponential (or Gaussian) kernel

$$K(\mathbf{x}, \mathbf{x}') = \gamma \exp\left(-\sum_{j=1}^d \frac{(x_j - x'_j)^2}{2\eta_j^2}\right) \quad (1)$$

where $\gamma \in \mathbb{R}_+ := \{x \in \mathbb{R} : x > 0\}$ is a scaling parameter and $\boldsymbol{\eta} \in \mathbb{R}_+^d$ are per-dimension lengthscales. Other popular choices for K include the rational quadratic kernel and those in the Matérn family; see ([Rasmussen and Williams, 2006](#), Chapter 4), ([Fasshauer, 2007](#)), or ([Duvenaud, 2014](#), Chapter 2) for additional details on GP kernels. The fast GPs we present will require $\mathcal{X} = [0, 1]^d$ and will use product kernels of the form

$$K(\mathbf{x}, \mathbf{x}') = \gamma \prod_{j=1}^d \left[1 + \eta_j \mathcal{K}(x_j, x'_j)\right] \quad (2)$$

where $\mathcal{K} : [0, 1) \rightarrow \mathbb{R}$ is some univariate kernel. Note that in (1) $\boldsymbol{\eta}$ act as input scales, while in (2) $\boldsymbol{\eta}$ act as output scales.

Suppose we have n observations $\mathbf{y} = \mathbf{f} + \boldsymbol{\varepsilon}$ which we assume to be the sum of the true function observations $\mathbf{f} := (f(\mathbf{x}_i))_{i=0}^{n-1}$ at collocation points $\mathbf{X} := (\mathbf{x}_i)_{i=0}^{n-1} \in \mathcal{X}^n$ and some zero-mean IID Gaussian noise $\boldsymbol{\varepsilon} \sim \mathcal{N}(\mathbf{0}, \xi \mathbf{1}_n)$ with common noise variance (nugget) $\xi \geq 0$ where $\xi = 0$ corresponds to the noise-free case with $\boldsymbol{\varepsilon} = \mathbf{0}$. The posterior distribution of f given sampling locations \mathbf{X} and noisy observations \mathbf{y} is also a Gaussian process, $f|\mathbf{X}, \mathbf{y} \sim \text{GP}(\mathbb{E}[f|\mathbf{X}, \mathbf{y}], \text{Cov}[f, f|\mathbf{X}, \mathbf{y}])$, with the closed form posterior mean and variance

$$\mathbb{E}[f(\mathbf{x})|\mathbf{X}, \mathbf{y}] = \tau + \mathbf{K}^\top(\mathbf{x})\widetilde{\mathbf{K}}^{-1}(\mathbf{y} - \tau\mathbf{1}) \quad \text{and} \quad \text{Cov}[f(\mathbf{x}), f(\mathbf{x}')|\mathbf{X}] = K(\mathbf{x}, \mathbf{x}') - \mathbf{K}^\top(\mathbf{x})\widetilde{\mathbf{K}}^{-1}\mathbf{K}(\mathbf{x}') \quad (3)$$

respectively. Here $\mathbf{K}(\mathbf{x}) := (K(\mathbf{x}, \mathbf{x}_i))_{i=0}^{n-1} \in \mathbb{R}^n$ is a vector of kernel evaluations and $\widetilde{\mathbf{K}} := \mathbf{K} + \xi \mathbf{1}_n \in \mathbb{R}^{n \times n}$ is the noisy version of the SPD Gram matrix $\mathbf{K} := (K(\mathbf{x}_i, \mathbf{x}_{i'}))_{i, i'=0}^{n-1} \in \mathbb{R}^{n \times n}$. Notice the posterior covariance in (3) only depends on the sampling locations \mathbf{X} and kernel K , not the noisy evaluations \mathbf{y} .

The GP typically relies on hyperparameters $\boldsymbol{\theta}$, e.g., $\boldsymbol{\theta} = \{\tau, \gamma, \boldsymbol{\eta}, \xi\}$, which are usually chosen to minimize some loss function. Perhaps the most popular optimization objective is the negative marginal log-likelihood (NMLL) loss, which, up to an additive constant independent of $\boldsymbol{\theta}$, is proportional to

$$\mathcal{L}_{\text{NMLL}}(\boldsymbol{\theta}) := (\mathbf{y} - \tau\mathbf{1})^\top \widetilde{\mathbf{K}}^{-1}(\mathbf{y} - \tau\mathbf{1}) + \log|\widetilde{\mathbf{K}}|. \quad (4)$$

Another popular optimization objective is the generalized cross validation (GCV) loss which is proportional to

$$\mathcal{L}_{\text{GCV}}(\boldsymbol{\theta}) := \frac{(\mathbf{y} - \tau\mathbf{1})^\top \widetilde{\mathbf{K}}^{-2}(\mathbf{y} - \tau\mathbf{1})}{(\text{trace}(\widetilde{\mathbf{K}}^{-1}))^2}. \quad (5)$$

In both (4) and (5) we have hidden the implicit dependence of $\widetilde{\mathbf{K}}$ on $\boldsymbol{\theta}$. The following theorem is a well known result which gives optimal choices for the constant prior mean τ under either of the above loss functions.

Theorem 2.1 (GP optimal constant prior means). *The NMLL loss (4) and GCV loss (5) are minimized when the prior mean is respectively*

$$\tau_{\text{NMLL}} = \frac{\mathbf{1}^\top \widetilde{\mathbf{K}}^{-1} \mathbf{y}}{\mathbf{1}^\top \widetilde{\mathbf{K}}^{-1} \mathbf{1}} \quad \text{and} \quad \tau_{\text{GCV}} = \frac{\mathbf{1}^\top \widetilde{\mathbf{K}}^{-2} \mathbf{y}}{\mathbf{1}^\top \widetilde{\mathbf{K}}^{-2} \mathbf{1}}. \quad (6)$$

The computational bottlenecks for GPs are the requirements to solve linear systems in the noisy SPD Gram matrix $\widetilde{\mathbf{K}}$ and to compute the determinant $|\widetilde{\mathbf{K}}|$ if evaluating the NMLL loss (4). Standard practice is to compute the Cholesky decomposition of $\widetilde{\mathbf{K}}$, which requires $\mathcal{O}(n^3)$ computations, and then solve the linear systems with back-substitution solves at cost $\mathcal{O}(n^2)$ and compute the determinant at cost $\mathcal{O}(n)$. Inference of the posterior mean and posterior covariance in (3) can then be performed at $\mathcal{O}(n)$ and $\mathcal{O}(n^2)$ cost respectively. Table 1 lists the computation and storage requirements, assuming K costs $\mathcal{O}(d)$ to evaluate as we will assume throughout this article.

	computations		storage	
	GP	fast GP	GP	fast GP
single-task	$n^3 + n^2d$	$n \log n + nd$	n^2	n
multitask equal	$n^3L^3 + n^2L^2d$	$(n \log n)L^2 + nL^3 + nL^2d$	n^2L^2	nL^2
multitask unequal	$N^3 + N^2d$	$\sum_{\ell=1}^L (L - \ell + 1)(n_\ell \log n_\ell + dn_\ell) + \sum_{\ell=2}^L (\sum_{\ell'=1}^{\ell-1} n_{\ell'})^2 / n_\ell + N^2 / n_L$	N^2	$\sum_{\ell=1}^L (L - \ell + 1)n_\ell + N^2 / n_L$

Table 1: Comparison of cost and storage requirements for fitting GPs, including hyperparameter optimization to minimize the NMLL loss in (4) or the GCV loss in (5). The “multitask unequal” setting allows for an arbitrary $L \in \mathbb{N}$ tasks with any $n_1, \dots, n_L \in \mathbb{N}$ assumed to be ordered so that $n_1 \geq \dots \geq n_L$. The “multitask equal” setting has arbitrary $L \in \mathbb{N}$ but assumes $n_1 = n_2 = \dots = n_L := n$. “Single-task” has $L = 1$ and $n_1 := n$. The fast GP constructions require that for $n_\ell = 2^{m_\ell}$ for some $m_\ell \in \mathbb{N}_0$ for all $\ell \in \{1, \dots, L\}$.

We will also consider Bayesian cubature for the mean

$$\mu := \int_{\mathcal{X}} f(\mathbf{x}) d\mathbf{x} \mid \mathcal{X}, \mathbf{y} \sim \mathcal{N}(\widehat{\mu}, \sigma^2) \quad (7)$$

where $\widehat{\mu} := \int_{\mathcal{X}} \mathbb{E}[f(\mathbf{x}) \mid \mathcal{X}, \mathbf{y}] d\mathbf{x}$ and $\sigma^2 := \int_{\mathcal{X}} \int_{\mathcal{X}} \text{Cov}[f(\mathbf{x}), f(\mathbf{x}') \mid \mathcal{X}] d\mathbf{x} d\mathbf{x}'$.

2.2. Fast Gaussian Processes

We will consider two types of fast GPs pairing special kernels with certain low-discrepancy (LD) sequences in $\mathcal{X} = [0, 1)^d$:

1. Fast GPs pairing LD shifted rank-1 lattices $(\mathbf{x}_i)_{i \in \mathbb{N}_0}$ in the extensible radical-inverse order (Definition 2.2) with shift-invariant (SI) kernels K (Definition 2.3). This creates Gram matrices \widetilde{K} whose eigenvectors are a bit-reversal permutation matrix times the inverse discrete Fourier matrix. All computations can be done at $O(n \log n)$ cost using the fast Fourier transforms (FFTs) (Cooley and Tukey, 1965).
2. Fast GPs pairing LD digitally-shifted base-2 digital sequences $(\mathbf{x}_i)_{i \in \mathbb{N}_0}$ in the extensible radical-inverse order (Definition 2.5) with digitally-shift-invariant (DSI) kernels K (Definition 2.6). This creates Gram matrices K whose eigenvectors are the Hadamard matrix. All computations can be done at $O(n \log n)$ cost using fast Walsh–Hadamard transforms (FWHTs) (Fino and Algazi, 1976).

These fast GPs were originally developed in (Zeng et al., 2009, 2006) and have found recent applications in (Rathinavel and Hickernell, 2019, 2022; Rathinavel, 2019; Kaarnioja et al., 2022, 2023; Sorokin et al., 2025b; Sorokin, 2025a; Sorokin et al., 2025a, 2024). Figure 1 shows the uniform coverage of these LD sequences contrasted against the gaps and clusters of independent points

First, let us define shifted rank-1 lattices and SI kernels.

Definition 2.2 (Shifted rank-1 lattice). *For a fixed generating vector $\mathbf{g} \in \mathbb{N}^d$, the rank-1 lattice $(\mathbf{z}_i)_{i \geq 0} \subset [0, 1)^d$ in radical-inverse order sets $\mathbf{z}_i = v(i)\mathbf{g} \bmod 1$ where $v(i)$ is the van der Corput sequence (van der Corput, 1935) with $v(0) = 0$ and $v(i) = \sum_{p=0}^{\lfloor \log_2(i) \rfloor} i_p 2^{-p-1}$ for $i = \sum_{p=0}^{\lfloor \log_2(i) \rfloor} i_p 2^p$. For a shift $\Delta \in [0, 1)^d$, the shifted rank-1 lattice $(\mathbf{x}_i)_{i \geq 0}$ sets $\mathbf{x}_i = (\mathbf{z}_i + \Delta) \bmod 1$.*

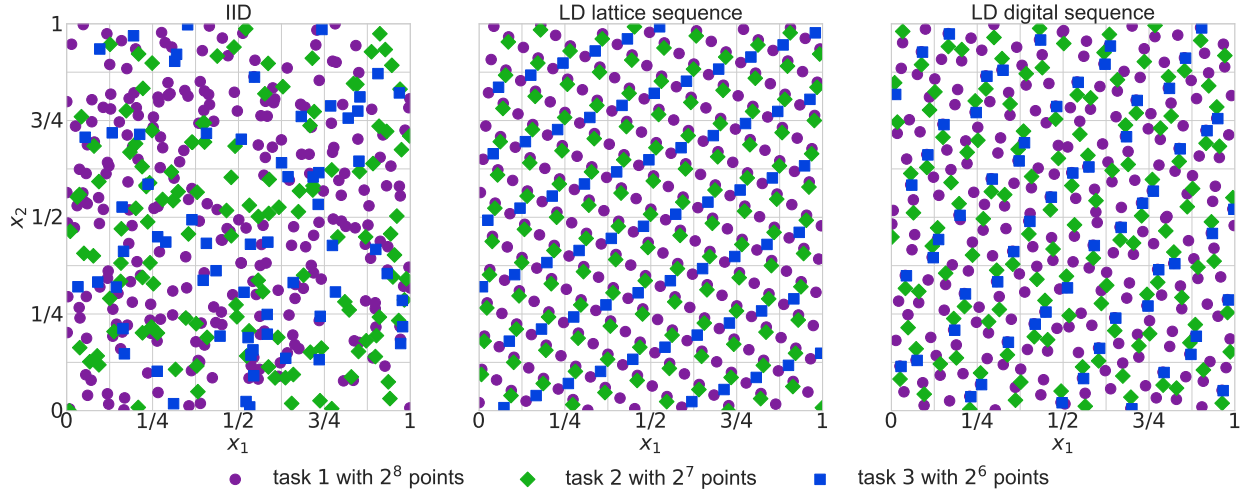


Figure 1: Independent identically distributed (IID) and low-discrepancy (LD) sequences. Each sequence has three independent randomizations shown in different colors, one for each task. The LD lattice has three independent uniform random shifts while the LD digital sequence has three independent uniform random digital-shifts. Different numbers of points are used for different tasks. Notice the more uniform coverage of LD sequences compared to IID points.

Definition 2.3 (Shift-invariant kernel). *A kernel $K : [0, 1)^d \times [0, 1)^d \rightarrow \mathbb{R}$ is SI when $K(\mathbf{x}, \mathbf{x}') = \widehat{K}((\mathbf{x} - \mathbf{x}') \bmod 1)$ for some $\widehat{K} : [0, 1)^d \rightarrow \mathbb{R}$ and any $\mathbf{x}, \mathbf{x}' \in [0, 1)^d$.*

One popular class of SI kernels take the product form in (2) with univariate kernels

$$\mathcal{K}(\mathbf{x}, \mathbf{x}') = \frac{(-1)^{\alpha+1} (2\pi)^{2\alpha}}{(2\alpha)!} B_{2\alpha}((\mathbf{x} - \mathbf{x}') \bmod 1) \quad (8)$$

where $\alpha \in \mathbb{N}$ is a smoothness parameter and B_p denotes the p -th Bernoulli polynomial. Such kernels have been extensively studied throughout the QMC literature (Kaarnioja et al., 2022, 2023; Cools et al., 2021, 2020; Sloan and Woźniakowski, 2001; Kuo et al., 2004).

Next, let us define the required digitally-shifted digital sequences and DSI kernels which will both depend on the digital-shift operator \oplus . In the following definitions we assume binary expansions do not end in an infinite tail of ones.

Definition 2.4 (Digital-shift operator \oplus). *For scalars $a, b \in [0, 1)$ with binary expansions $a = \sum_{p \in \mathbb{N}_0} \mathbf{a}_p 2^{-p}$ and $b = \sum_{p \in \mathbb{N}_0} \mathbf{b}_p 2^{-p}$, we set $a \oplus b = \sum_{p \in \mathbb{N}_0} ((\mathbf{a}_p + \mathbf{b}_p) \bmod 2) 2^{-p}$ to be the exclusive or (XOR) between binary digits. For vectors $\mathbf{a}, \mathbf{b} \in [0, 1)^d$, we set $\mathbf{a} \oplus \mathbf{b} := (a_1 \oplus b_1, \dots, a_d \oplus b_d)$ to act elementwise.*

Definition 2.5 (Base-2 digitally-shifted digital sequences). *For generating matrices $\mathbf{G} \in [0, 1)^{d \times \infty}$ with zeroth column \mathbf{g}_0 and p -th column \mathbf{g}_p , the digital sequence $(\mathbf{z}_i)_{i \geq 0} \subset [0, 1)^d$ in radical-inverse order sets $\mathbf{z}_i = \bigoplus_{p=0}^{\lfloor \log_2(i) \rfloor} i_p \mathbf{g}_p$. For a digital-shift $\Delta \in [0, 1)^d$, the digitally-shifted digital sequence $(\mathbf{x}_i)_{i \geq 0}$ sets $\mathbf{x}_i = \mathbf{z}_i \oplus \Delta$.*

Definition 2.6 (Digitally-shift-invariant kernel). A kernel $K : [0, 1)^d \times [0, 1)^d \rightarrow \mathbb{R}$ is DSI when $K(\mathbf{x}, \mathbf{x}') = \widehat{K}(\mathbf{x} \oplus \mathbf{x}')$ for some $\widehat{K} : [0, 1)^d \rightarrow \mathbb{R}$ and any $\mathbf{x}, \mathbf{x}' \in [0, 1)^d$.

Sorokin et al. (2025a) recently proposed an adaptive-smoothness DSI product kernel in the form of (2) where

$$\mathcal{K}(\mathbf{x}, \mathbf{x}') = b_1 \widehat{\mathcal{K}}_1(\mathbf{x} \oplus \mathbf{x}') + b_2 \widehat{\mathcal{K}}_2(\mathbf{x} \oplus \mathbf{x}') + b_3 \widehat{\mathcal{K}}_3(\mathbf{x} \oplus \mathbf{x}') + b_4 \widehat{\mathcal{K}}_4(\mathbf{x} \oplus \mathbf{x}') \quad \text{with}$$

$$\widehat{\mathcal{K}}_\alpha(x) = \begin{cases} 6\left(1 - \frac{1}{2}t_1(x)\right), & \alpha = 1 \\ -1 + -\beta(x)x + \frac{5}{2}[1 - t_1(x)], & \alpha = 2 \\ -1 + \beta(x)x^2 - 5[1 - t_1(x)]x + \frac{43}{18}[1 - t_2(x)], & \alpha = 3 \\ -1 - \frac{2}{3}\beta(x)x^3 + 5[1 - t_1(x)]x^2 - \frac{43}{9}[1 - t_2(x)]x \\ \quad + \frac{701}{294}[1 - t_3(x)] + \beta(x)\left[\frac{1}{48}\sum_{a=1}^{\infty}\frac{x_a}{2^{3(a-1)}} - \frac{1}{42}\right], & \alpha = 4 \end{cases} \quad (9)$$

Here $\beta(x) = -\lceil \log_2(x) \rceil$, $t_\nu(x) = 2^{-\nu\beta(x)}$, and $\mathbf{b} \in \mathbb{R}_+^4$ are hyperparameter weights to be optimized. α is again a smoothness parameter with the above $\alpha = 1$ form due to Dick and Pillichshammer (2005), and the higher-order $\alpha \geq 2$ forms are due to Sorokin (2025b) with some recent numerical experiments given by Sorokin et al. (2025b). Despite having discontinuous kernels, the reproducing kernel Hilbert spaces (RKHSs) corresponding to the $\alpha \geq 2$ forms contain Sobolev spaces of smooth, non-periodic functions.

The following results from (Rathinavel, 2019) summarizes the two pairings discussed at the beginning of this section and fast computations they enable. Table 1 summarizes the resulting computations and storage requirements.

Condition 2.1 (Fast GP). Suppose $\mathcal{X} = [0, 1)^d$, $n = 2^m$ for some $m \in \mathbb{N}_0$, and either

1. (SI-LAT) K is SI (Definition 2.3) and \mathcal{X} is a shifted rank-1 lattice in radical-inverse order (Definition 2.2), or
2. (DSI-DSEQ) K is DSI (Definition 2.6) and \mathcal{X} is a digitally-shifted base-2 digital sequence in radical inverse order (Definition 2.5).

Theorem 2.2 (Fast GP computations). Under Condition 2.1, we have the eigendecomposition $\widetilde{K} = \mathbf{V}\widetilde{\Lambda}\mathbf{V}$ and:

1. \mathbf{V} is symmetric, unitary, and has the constant zeroth column $\mathbf{V}_{:,0} = \mathbf{1}/\sqrt{2^m}$.
2. Computing $\mathbf{V}\mathbf{a}$, $\widetilde{\mathbf{V}}\mathbf{a}$, $\widetilde{\mathbf{K}}\mathbf{a}$, $\widetilde{\mathbf{K}}^{-1}\mathbf{a}$, and $|\widetilde{\mathbf{K}}|$ for any $\mathbf{a} \in \mathbb{C}^n$ each cost $\mathcal{O}(2^m m)$.
3. $\widetilde{\boldsymbol{\lambda}} := \widetilde{\Lambda}\mathbf{1} = \sqrt{n}\widetilde{\mathbf{V}}\widetilde{\mathbf{K}}_{:,0}$ where $\widetilde{\mathbf{K}}_{:,0}$ is the zeroth column of $\widetilde{\mathbf{K}}$.
4. $\tau_{\text{NMLL}} = \tau_{\text{GCV}} = \mathbf{1}^\top \mathbf{y}/n$ in (6), i.e., in Theorem 2.1 the optimal constant prior means are the sample means.

For the SI-LAT condition, $\widetilde{\mathbf{V}}\mathbf{a}$ applies a bit-reversal permutation to \mathbf{a} then applies an FFT to the result. For the DSI-DSEQ condition, $\widetilde{\mathbf{V}}\mathbf{a}$ applies a FWHT \mathbf{a} and \mathbf{V} is real so $\widetilde{\mathbf{V}} = \mathbf{V}$.

Condition 2.2 (Fast Bayesian cubature). For some $\gamma \in \mathbb{R}_+$, $\int_{[0,1)^d} K(\mathbf{x}, \mathbf{x}')d\mathbf{x}' = \gamma$ holds for all $\mathbf{x} \in [0, 1)^d$.

Lemma 2.1. *Condition 2.2 is satisfied for product kernels of the form in (2) whenever $\int_0^1 \mathcal{K}(x, x') dx' = 0$ for all $x \in [0, 1)$. Moreover, Condition 2.2 holds for both the SI product kernel with \mathcal{K} in (8) and the DSI product kernel with \mathcal{K} in (9).*

Theorem 2.3 (Fast Bayesian cubature). *Suppose Condition 2.1 and Condition 2.2 are satisfied with $\tau = \tau_{\text{NMLL}} = \mathbf{1}^\top \mathbf{y}/n$ or $\tau = \tau_{\text{GCV}} = \mathbf{1}^\top \mathbf{y}/n$. Then $\widehat{\mu} = \mathbf{1}^\top \mathbf{y}/n$ and $\sigma^2 = \gamma - \gamma^2(\mathbf{1}^\top \widetilde{\mathbf{K}}_{:,0}/n)^{-1}$ in (7).*

2.3. Multitask Gaussian Processes

Suppose we have L tasks (levels), each acting on $\mathcal{X} \subseteq \mathbb{R}^d$. We will denote this set of functions by $f : \{1, \dots, L\} \times \mathcal{X} \rightarrow \mathbb{R}$, where $f(\ell, \mathbf{x})$ evaluates task $\ell \in \{1, \dots, L\}$ at parameters $\mathbf{x} \in \mathcal{X}$. Rather than fitting independent GPs to $f(1, \cdot), \dots, f(L, \cdot)$, we would like to fit a single GP which additionally exploits covariance information between tasks.

Let us assume f is a multitask GP (MTGP) on $\mathcal{X} \times \{1, \dots, L\}$ with prior mean constants $\boldsymbol{\tau} \in \mathbb{R}^L$ and a covariance kernel $K : (\{1, \dots, L\} \times \mathcal{X}) \times (\{1, \dots, L\} \times \mathcal{X}) \rightarrow \mathbb{R}$. Then $f \sim \text{GP}(\mathbb{E}[f], \text{Cov}[f, f])$ where the prior mean is $\mathbb{E}[f(\ell, \mathbf{x})] = \tau_\ell$ and the prior covariance is $\text{Cov}[f(\ell, \mathbf{x}), f(\ell', \mathbf{x}')] = K((\ell, \mathbf{x}), (\ell', \mathbf{x}'))$ for all $\ell, \ell' \in \{1, \dots, L\}$ and $\mathbf{x}, \mathbf{x}' \in \mathcal{X}$.

Suppose we have $N = \sum_{\ell=1}^L n_\ell$ total observations where for task $\ell \in \{1, \dots, L\}$ we observe $\mathbf{y}_\ell = \mathbf{f}_\ell + \boldsymbol{\varepsilon}_\ell$ which we again assume to be the sum of the true function observations $\mathbf{f}_\ell = (f(\ell, \mathbf{x}_{\ell i}))_{i=0}^{n_\ell-1}$ at collocation points $\mathbf{X}_\ell := (\mathbf{x}_{\ell i})_{i=0}^{n_\ell-1} \subset \mathcal{X}^{n_\ell}$ and some zero-mean IID Gaussian noise $\boldsymbol{\varepsilon}_\ell \sim \mathcal{N}(\mathbf{0}, \xi_\ell \mathbf{1}_{n_\ell})$ with common noise variance (nugget) $\xi_\ell \geq 0$ where $\xi_\ell = 0$ corresponds to the noise-free case with $\boldsymbol{\varepsilon}_\ell = \mathbf{0}$. We also assume $\boldsymbol{\varepsilon}_1, \dots, \boldsymbol{\varepsilon}_L$ are independent.

The posterior distribution of f given sampling locations $\mathbf{X} := (\mathbf{X}_\ell)_{\ell=1}^L \in \mathcal{X}^N$ and noisy observations $\mathbf{y} = (\mathbf{y}_\ell)_{\ell=1}^L \in \mathbb{R}^N$ is also a Gaussian process, $f|\mathbf{X}, \mathbf{y} \sim \text{GP}(\mathbb{E}[f|\mathbf{X}, \mathbf{y}], \text{Cov}[f, f|\mathbf{X}, \mathbf{y}])$, with the closed form posterior mean and variance

$$\begin{aligned} \mathbb{E}[f(\ell, \mathbf{x})|\mathbf{X}, \mathbf{y}] &= \tau_\ell + \mathbf{K}^\top(\ell, \mathbf{x})\widetilde{\mathbf{K}}^{-1}(\mathbf{y} - \mathbf{E}\boldsymbol{\tau}) \quad \text{and} \\ \text{Cov}[f(\ell, \mathbf{x}), f(\ell', \mathbf{x}')|\mathbf{X}] &= K((\ell, \mathbf{x}), (\ell', \mathbf{x}')) - \mathbf{K}^\top(\ell, \mathbf{x})\widetilde{\mathbf{K}}^{-1}\mathbf{K}(\ell', \mathbf{x}') \end{aligned} \quad (10)$$

respectively. Here $\mathbf{K}(\ell, \mathbf{x}) := (\mathbf{K}_{\ell'}(\ell, \mathbf{x}))_{\ell'=1}^L \in \mathbb{R}^N$ for $\mathbf{K}_{\ell'}(\ell, \mathbf{x}) := (K((\ell, \mathbf{x}), (\ell', \mathbf{x}_{\ell' i})))_{i=0}^{n_{\ell'}-1} \in \mathbb{R}^{n_{\ell'}}$, and $\widetilde{\mathbf{K}} := (\widetilde{\mathbf{K}}_{\ell\ell'})_{\ell, \ell'=1}^L \in \mathbb{R}^{N \times N}$ for $\widetilde{\mathbf{K}}_{\ell\ell'} := \mathbf{K}_{\ell\ell'} + \delta_{\ell\ell'} \xi_{\ell'} \mathbf{1}_{n_{\ell'}} \in \mathbb{R}^{n_{\ell} \times n_{\ell'}}$ where $\mathbf{K}_{\ell\ell'} := (K((\ell, \mathbf{x}_{\ell i}), (\ell', \mathbf{x}_{\ell' i'})))_{i, i'=0}^{n_{\ell}-1, n_{\ell'}-1} \in \mathbb{R}^{n_{\ell} \times n_{\ell'}}$ with the delta function $\delta_{\ell\ell'}$ equal to 1 if $\ell = \ell'$ and 0 otherwise. Moreover, we have used the ‘‘task-summing’’ matrix

$$\mathbf{E} = \begin{pmatrix} \mathbf{1}_1 & & \\ & \ddots & \\ & & \mathbf{1}_L \end{pmatrix} \in \mathbb{R}^{N \times L}, \quad \text{e.g., for } L = 2, n_1 = 2, \text{ and } n_2 = 3 \text{ we have } \mathbf{E} = \begin{pmatrix} 1 & 0 \\ 1 & 0 \\ 0 & 1 \\ 0 & 1 \\ 0 & 1 \end{pmatrix} \in \mathbb{R}^{5 \times 2}.$$

The NMLL loss in (4) and the GCV loss in (5) for MTGPs are respectively

$$\mathcal{L}_{\text{NMLL}}(\boldsymbol{\theta}) := (\mathbf{y} - \mathbf{E}\boldsymbol{\tau})^\top \widetilde{\mathbf{K}}^{-1}(\mathbf{y} - \mathbf{E}\boldsymbol{\tau}) + \log|\widetilde{\mathbf{K}}| \quad \text{and} \quad \mathcal{L}_{\text{GCV}}(\boldsymbol{\theta}) := \frac{(\mathbf{y} - \mathbf{E}\boldsymbol{\tau})^\top \widetilde{\mathbf{K}}^{-2}(\mathbf{y} - \mathbf{E}\boldsymbol{\tau})}{\text{trace}^2(\widetilde{\mathbf{K}}^{-1})}. \quad (11)$$

The following theorem gives optimal choices for the constant prior means $\boldsymbol{\tau}$ under either of the above loss functions

Theorem 2.4 (MTGP optimal constant prior means). *The MTGP NMLL loss (11) and GCV loss (11) are minimized when the prior means respectively satisfy*

$$(\mathbf{E}^\top \widetilde{\mathbf{K}}^{-1} \mathbf{E}) \boldsymbol{\tau}_{\text{NMLL}} = \mathbf{E}^\top \widetilde{\mathbf{K}}^{-1} \mathbf{y} \quad \text{and} \quad (\mathbf{E}^\top \widetilde{\mathbf{K}}^{-2} \mathbf{E}) \boldsymbol{\tau}_{\text{GCV}} = \mathbf{E}^\top \widetilde{\mathbf{K}}^{-2} \mathbf{y}. \quad (12)$$

The computational and storage requirements for MTGPs are completely analogous to the GP case, see [Table 1](#).

For multitask Bayesian cubature, we have

$$\boldsymbol{\mu} := \left(\int_{\mathcal{X}} f(\ell, \mathbf{x}) d\mathbf{x} \right)_{\ell=1}^L \Big| \mathcal{X}, \mathbf{y} \sim \mathcal{N}(\widehat{\boldsymbol{\mu}}, \boldsymbol{\Sigma}) \quad (13)$$

where $\widehat{\boldsymbol{\mu}} := \left(\int_{\mathcal{X}} \mathbb{E}[f(\ell, \mathbf{x}) | \mathcal{X}, \mathbf{y}] d\mathbf{x} \right)_{\ell=1}^L \in \mathbb{R}^L$ and $\boldsymbol{\Sigma} := \left(\int_{\mathcal{X}} \int_{\mathcal{X}} \text{Cov}[f(\ell, \mathbf{x}), f(\ell', \mathbf{x}') | \mathcal{X}] d\mathbf{x} d\mathbf{x}' \right)_{\ell, \ell'=1}^L \in \mathbb{R}^{L \times L}$. We are often interested in a linear combination of integrals for each task. Suppose we have user-provided weights $\boldsymbol{\chi} \in \mathbb{R}^L$ for which our quantity of interest is $\boldsymbol{\chi}^\top \boldsymbol{\mu} \sim \mathcal{N}(\boldsymbol{\chi}^\top \widehat{\boldsymbol{\mu}}, \boldsymbol{\chi}^\top \boldsymbol{\Sigma} \boldsymbol{\chi})$, e.g., $\boldsymbol{\chi} = (0, \dots, 0, 1)^\top$ to select the final task mean or $\boldsymbol{\chi} = \mathbf{1}$ if $f(\ell, \mathbf{x})$ models the difference of consecutive fidelity levels as in multilevel (Q)MC ([Giles, 2008](#); [Giles and Waterhouse, 2009](#); [Giles, 2015](#); [Sorokin et al., 2025a](#)). [Section Appendix A](#) derives an optimal reweighing to minimize the MSE of the multitask Bayesian cubature estimate, although we did not consider this in our numerical experiments.

Remark 2.1 (Derivative informed GPs). *Suppose we have L compatible derivative multi-indices $\boldsymbol{\beta}_1, \dots, \boldsymbol{\beta}_L \in \mathbb{N}_0^d$, and we observe for task $\ell \in \{1, \dots, L\}$ noise-free derivative observations $\mathbf{y}_\ell = f^{(\boldsymbol{\beta}_\ell)} + \boldsymbol{\varepsilon}_\ell$ where $f^{(\boldsymbol{\beta})} := \partial_{x_1}^{\beta_1} \dots \partial_{x_d}^{\beta_d} f(\mathbf{x})$ for $\boldsymbol{\beta} \in \mathbb{N}_0^d$. Then derivative-informed GPs may be seen as a special case of MTGPs with a kernel $K((\ell, \mathbf{x}), (\ell', \mathbf{x}')) := K^{(\boldsymbol{\beta}_\ell, \boldsymbol{\beta}_{\ell'})}(\mathbf{x}, \mathbf{x}')$ where $K^{(\boldsymbol{\beta}, \boldsymbol{\beta}')}(\mathbf{x}, \mathbf{x}') := \partial_{x_1}^{\beta_1} \dots \partial_{x_d}^{\beta_d} \partial_{x'_1}^{\beta'_1} \dots \partial_{x'_d}^{\beta'_d} K(\mathbf{x}, \mathbf{x}')$ for $\boldsymbol{\beta}, \boldsymbol{\beta}' \in \mathbb{N}_0^d$. Note that this requires suitable assumptions on the derivatives of the kernel and the distribution of the noise as well as a natural modification to the posterior mean. ([Rasmussen and Williams, 2006, Chapter 9.4](#)), ([Wendland, 2004, Chapter 16](#)), ([Banerjee et al., 2003](#)), and ([Owhadi and Scovel, 2019](#)) discuss generalized GPs formulations as optimal recovery problems in Hilbert spaces, while ([Eriksson et al., 2018](#); [Solak et al., 2002](#); [Wu et al., 2017](#); [Padidar et al., 2021](#); [Sorokin et al., 2025b](#)) given applications of derivative-informed GPs.*

2.4. Fast Multitask Gaussian Processes

Fast MTGPs use multitask product kernels which are ubiquitous in the MTGPs literature ([Bonilla et al., 2007](#)).

Definition 2.7 (Multitask product kernel). *$K : (\{1, \dots, L\} \times \mathcal{X}) \times (\{1, \dots, L\} \times \mathcal{X}) \rightarrow \mathbb{R}$ is a multitask product kernel with task kernel $R : \{1, \dots, L\} \times \{1, \dots, L\} \rightarrow \mathbb{R}$ and spatial kernel $Q : \mathcal{X} \times \mathcal{X} \rightarrow \mathbb{R}$ if $K((\ell, \mathbf{x}), (\ell', \mathbf{x}')) = R(\ell, \ell') Q(\mathbf{x}, \mathbf{x}')$ for all $\ell, \ell' \in \{1, \dots, L\}$ and all $\mathbf{x}, \mathbf{x}' \in \mathcal{X}$.*

As with fast GPs, fast MTGPs will require $\mathcal{X} = [0, 1)^d$. The kernel R is typically parameterized directly by a low rank matrix $\mathbf{B} \in \mathbb{R}^{L \times s}$ with $s \in \{0, \dots, L\}$ and a diagonal vector $\mathbf{t} \in \mathbb{R}_+^L$ so that the task Gram matrix is $\mathbf{R} := (R(\ell, \ell'))_{\ell, \ell'=1}^L = \mathbf{B} \mathbf{B}^\top + \text{diag}(\mathbf{t})$.

Condition 2.3 (Fast MTGP). Suppose $\mathcal{X} = [0, 1]^d$ and $K : (\{1, \dots, L\} \times [0, 1]^d) \times (\{1, \dots, L\} \times [0, 1]^d) \rightarrow \mathbb{R}$ is a multitask product kernel with task kernel $R : \{1, \dots, L\} \times \{1, \dots, L\}$ and spatial kernel $Q : [0, 1]^d \times [0, 1]^d \rightarrow \mathbb{R}$. Suppose $n_\ell = 2^{m_\ell}$ for some $m_\ell \in \mathbb{N}_0$ for all $\ell \in \{1, \dots, L\}$, and assume $n_1 \geq \dots \geq n_L$, which may always be satisfied by reindexing tasks. Suppose either

1. **(SI-LAT)** Q is SI (Definition 2.3) and $\mathbf{X}_1, \dots, \mathbf{X}_\ell$ are shifted rank-1 lattices in radical-inverse order (Definition 2.2) with a common generating vector $\mathbf{g} \in \mathbb{N}_0^d$ and possibly different shifts per task, i.e., $\mathbf{x}_{\ell i} = (v(i)\mathbf{g} + \Delta_\ell) \bmod 1$ for some $\Delta_1, \dots, \Delta_L \in [0, 1]^d$, or
2. **(DSI-DSEQ)** Q is DSI (Definition 2.6) and $\mathbf{X}_1, \dots, \mathbf{X}_\ell$ are digitally-shifted base-2 digital nets in radical-inverse order (Definition 2.5) with common generating matrices $\mathbf{G} \in [0, 1]^{d \times \infty}$ and possibly different digital-shifts per task, i.e., $\mathbf{x}_{\ell i} = \bigoplus_{p=0}^{\lfloor \log_2(i) \rfloor} i_p \mathbf{g}_p \oplus \Delta_\ell$ for some $\Delta_1, \dots, \Delta_L \in [0, 1]^d$.

Figure 1 visualizes such lattice and digital sequences for an $L = 3$ task setup with random shifts $\Delta_1, \dots, \Delta_L \sim \mathcal{U}[0, 1]^d$ and differing numbers of points per task. The following theorem summarizes structures and results derived in (Sorokin, 2025a, Chapter 5.2).

Theorem 2.5 (Fast MTGP computations). Under Condition 2.3, we have the decomposition $\widetilde{\mathbf{K}}_{\ell\ell'} = \mathbf{V}_{m_\ell} \widetilde{\Lambda}_{\ell\ell'} \overline{\mathbf{V}}_{m_{\ell'}}$ in $\mathbb{R}^{2^{m_\ell} \times 2^{m_{\ell'}}}$, where, for all $m \in \mathbb{N}_0$,

1. $\mathbf{V}_m \in \mathbb{C}^{2^m \times 2^m}$ is symmetric, unitary, and has the constant zeroth column $(\mathbf{V}_m)_{:,0} \mathbf{1} / \sqrt{2^m}$.
2. Computing $\mathbf{V}_m \mathbf{a}$ and $\overline{\mathbf{V}}_m \mathbf{a}$ for any $\mathbf{a} \in \mathbb{C}^{2^m}$ each cost $\mathcal{O}(2^m m)$.
3. Regarding $\Lambda_{\ell\ell'} \in \mathbb{C}^{2^{m_\ell} \times 2^{m_{\ell'}}}$,
 - (tall-case) if $m_\ell \geq m_{\ell'}$ then $\widetilde{\Lambda}_{\ell\ell'}$ is a $2^{m_\ell - m_{\ell'}} \times 1$ block matrix with $2^{m_{\ell'}} \times 2^{m_{\ell'}}$ diagonal blocks which is fully specified by $\widetilde{\lambda}_{\ell\ell'} := \widetilde{\Lambda}_{\ell\ell'} \mathbf{1} = \sqrt{2^{m_{\ell'}}} \overline{\mathbf{V}}_{m_{\ell'}} (\widetilde{\mathbf{K}}_{\ell\ell'})_{:,0}$ where $(\widetilde{\mathbf{K}}_{\ell\ell'})_{:,0}$ is the zeroth column of $\widetilde{\mathbf{K}}_{\ell\ell'}$, whereas
 - (wide-case) if $m_\ell \leq m_{\ell'}$ then $\widetilde{\Lambda}_{\ell\ell'}$ is a $1 \times 2^{m_{\ell'} - m_\ell}$ block matrix with $2^{m_\ell} \times 2^{m_\ell}$ diagonal blocks which is fully specified by $\widetilde{\lambda}_{\ell\ell'} := \mathbf{1}^\top \widetilde{\Lambda}_{\ell\ell'} = \sqrt{2^{m_\ell}} \mathbf{V}_{m_\ell} (\widetilde{\mathbf{K}}_{\ell\ell'})_{0,:}^\top$ where $(\widetilde{\mathbf{K}}_{\ell\ell'})_{0,:}$ is the zeroth row of $\widetilde{\mathbf{K}}_{\ell\ell'}$.

Under the SI-LAT condition, $\overline{\mathbf{V}}_m \mathbf{a}$ applies a bit-reversal permutation to \mathbf{a} then applies an FFT to the result. Under the DSI-DSEQ condition, $\mathbf{V}_m \mathbf{a}$ applies a FWHT to \mathbf{a} with real \mathbf{V}_m so $\overline{\mathbf{V}}_m = \mathbf{V}_m$.

To compute the inverse and determinant of $\widetilde{\mathbf{K}}$, it is sufficient to compute the inverse and determinant of the sparse matrix $\widetilde{\Lambda} := (\widetilde{\Lambda}_{\ell\ell'})_{\ell,\ell'=1}^L$ as $\widetilde{\mathbf{K}} = \mathbf{V} \widetilde{\Lambda} \overline{\mathbf{V}}$ where $\mathbf{V} := \text{diag}(\mathbf{V}_{m_1}, \dots, \mathbf{V}_{m_L})$ is a block diagonal matrix of fast transforms. We will use the notation $\widetilde{\Lambda}_{:\ell,:\ell'} := (\widetilde{\Lambda}_{\ell\ell'})_{\ell,\ell'=1}^{\ell,\ell'}$ to denote the first ℓ row blocks and first ℓ' column blocks, where of course $\widetilde{\Lambda}_{:L,:L} = \widetilde{\Lambda}$. We will also use $\widetilde{\Lambda}_{\ell,:\ell'} = (\widetilde{\Lambda}_{\ell\ell'})_{\ell'=1}^{\ell,\ell'}$ to denote the first ℓ' column blocks in the ℓ -th row, and use $\widetilde{\Lambda}_{:\ell,\ell} = (\widetilde{\Lambda}_{\ell\ell})_{\ell'=1}^{\ell,\ell}$ to denote the first ℓ' row blocks in the ℓ -th column. Let us also write $\widetilde{\Lambda}_{:\ell,:\ell}^{-1} := (\widetilde{\Lambda}_{:\ell,:\ell})^{-1}$ so $\widetilde{\Lambda}^{-1} = \widetilde{\Lambda}_{:L,:L}^{-1}$.

To motivate our fast inverse and determinant algorithm, let us consider an example with $L = 3$ tasks having $n_1 = 8$, $n_2 = 4$ and $n_3 = 2$. Figure 2 visualizes the resulting Gram matrix $\widetilde{\mathbf{K}}$ (in the DSI-DSEQ setting), the sparsity pattern of $\widetilde{\Lambda}$, and the $L = 3$ stage inversion algorithm. In the first

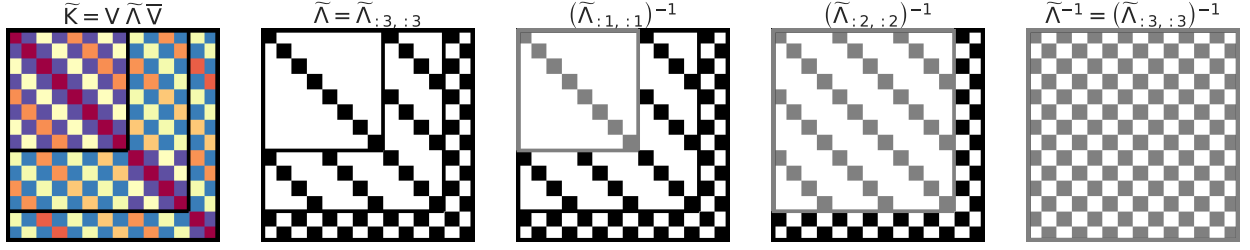


Figure 2: Structures and the inversion algorithm for an $L = 3$ fast MTGP with digital sequences and a digitally-shift-invariant kernel.

stage, we compute $\tilde{\Lambda}_{11}^{-1}$ which is simply the inverse of a diagonal matrix. In the second stage we compute

$$\tilde{\Lambda}_{:,2,:2}^{-1} = \begin{pmatrix} \tilde{\Lambda}_{11}^{-1} + \tilde{\Lambda}_{11}^{-1} \tilde{\Lambda}_{12} \mathbf{S}_2^{-1} \tilde{\Lambda}_{21} \tilde{\Lambda}_{11}^{-1} & -\tilde{\Lambda}_{11}^{-1} \tilde{\Lambda}_{12} \mathbf{S}_2^{-1} \\ -\mathbf{S}_2^{-1} \tilde{\Lambda}_{21} \tilde{\Lambda}_{11}^{-1} & \mathbf{S}_2^{-1} \end{pmatrix}$$

where $\mathbf{S}_2 = \tilde{\Lambda}_{22} - \tilde{\Lambda}_{21} \tilde{\Lambda}_{11}^{-1} \tilde{\Lambda}_{12}$ is the Schur complement. We also have that $|\tilde{\Lambda}_{:,2,:2}| = |\tilde{\Lambda}_{11}| \cdot |\mathbf{S}_2|$. In the third and final stage we compute

$$\tilde{\Lambda}^{-1} = \tilde{\Lambda}_{:,3,:3}^{-1} = \begin{pmatrix} \tilde{\Lambda}_{:,2,:2}^{-1} & \tilde{\Lambda}_{:,2,3} \\ \tilde{\Lambda}_{3,2} & \tilde{\Lambda}_{33} \end{pmatrix}^{-1} = \begin{pmatrix} \tilde{\Lambda}_{:,2,:2}^{-1} + \tilde{\Lambda}_{:,2,3} \mathbf{S}_3^{-1} \tilde{\Lambda}_{3,2} \tilde{\Lambda}_{:,2,:2}^{-1} & -\tilde{\Lambda}_{:,2,3} \mathbf{S}_3^{-1} \\ \mathbf{S}_3^{-1} \tilde{\Lambda}_{3,2} \tilde{\Lambda}_{:,2,:2}^{-1} & \mathbf{S}_3^{-1} \end{pmatrix}$$

where $\mathbf{S}_3 = \tilde{\Lambda}_{33} - \tilde{\Lambda}_{3,2} \tilde{\Lambda}_{:,2,:2}^{-1} \tilde{\Lambda}_{:,2,3}$ is another Schur complement and $|\tilde{\Lambda}| = |\tilde{\Lambda}_{:,3,:3}| = |\tilde{\Lambda}_{:,2,:2}| \cdot |\tilde{\Lambda}_{33}|$. Crucially, the Schur complements \mathbf{S}_ℓ are all diagonal and $\tilde{\Lambda}_{:, \ell, : \ell}^{-1}$ only depends on $\tilde{\Lambda}_{:, \ell-1, : \ell-1}^{-1}$, $\tilde{\Lambda}_{:, \ell-1, \ell}$, and $\tilde{\Lambda}_{\ell \ell}$.

Algorithm 1 generalizes the above routine for computing $\tilde{\Lambda}^{-1}$ and $|\tilde{\Lambda}|$ for arbitrary $L \in \mathbb{N}$. Then, **Theorem 2.6** analyzes the cost and storage requirements for computing $\tilde{\Lambda}$, multiplying by $\tilde{\mathbf{K}}$, inverting $\tilde{\mathbf{K}}$, and finding the determinant of $\tilde{\mathbf{K}}$. **Table 1** summarizes these cost and storage requirements.

Figure 3 visualizes the time-per optimization step for fast MTGP for an $L = 2$ task setup. Notice that, as expected, when the ratios n_1/n_2 or n_2/n_1 are high, the fast MTGPs take longer to fit. This is due to the greater sparsity in the matrix when these ratios are close to 1. For example, with $d = 100$, runtimes for $\mathbf{n} = (2^{15}, 2^6)^\top$ with $N = 32832$ are around $1e-0.75$ while runtimes for $\mathbf{n} = (2^{15}, 2^{15})^\top$ with $N = 65536$ are only $1e-0.85$ despite having almost twice as many total samples.

Theorem 2.6. Suppose **Condition 2.3** holds. Then evaluating $\tilde{\Lambda} \in \mathbb{C}^{N \times N}$ requires $\mathcal{O}\left(\sum_{\ell=1}^L (L - \ell + 1)(n_\ell \log n_\ell + dn_\ell)\right)$ computations and $\mathcal{O}\left(\sum_{\ell=1}^L (L - \ell + 1)n_\ell\right)$ storage. Having evaluated $\tilde{\Lambda}$, computing $\tilde{\mathbf{K}}\mathbf{y} = \mathbf{V}\tilde{\Lambda}\tilde{\mathbf{V}}\mathbf{y}$ for any $\mathbf{y} \in \mathbb{R}^N$ requires $\mathcal{O}\left(\sum_{\ell=1}^L n_\ell \log n_\ell + \sum_{\ell=1}^L (L - \ell + 1)n_\ell\right)$ computations. Having evaluated $\tilde{\Lambda}$, evaluating $|\tilde{\mathbf{K}}| = |\tilde{\Lambda}|$ and $\tilde{\Lambda}^{-1}$ using **Algorithm 1** requires $\mathcal{O}\left(\sum_{\ell=2}^L \left(\sum_{\ell'=1}^{\ell-1} n_{\ell'}\right)^2 / n_\ell\right)$ computations and $\mathcal{O}(N^2/n_L)$ storage. Having stored $\tilde{\Lambda}^{-1}$, evaluating $\tilde{\mathbf{K}}^{-1}\mathbf{y} = \mathbf{V}\tilde{\Lambda}^{-1}\tilde{\mathbf{V}}\mathbf{y}$ for any $\mathbf{y} \in \mathbb{R}^N$ requires $\mathcal{O}\left(\sum_{\ell=1}^L n_\ell \log n_\ell + N^2/n_L\right)$ computations.

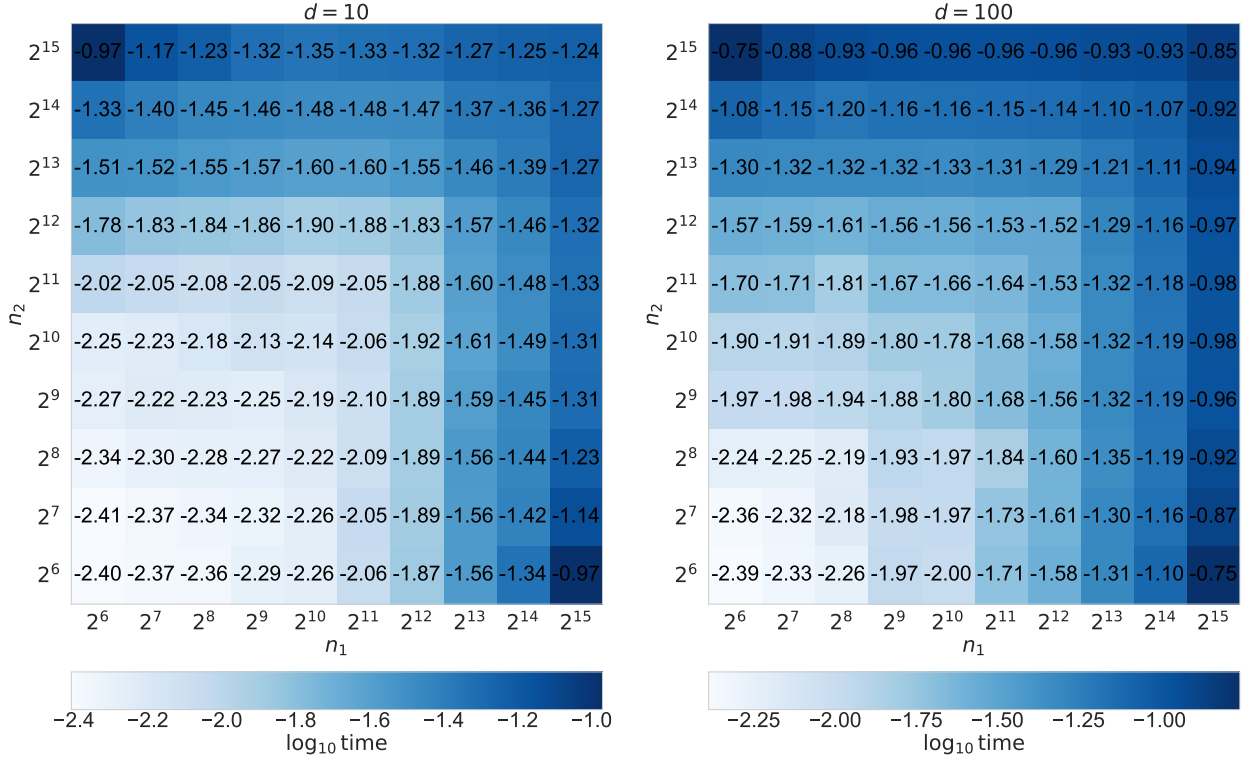


Figure 3: Time per optimization step of our fast MTGPs for $L = 2$ tasks.

Corollary 2.1. Suppose [Condition 2.3](#) holds for $n := n_\ell = 2^m$ with $m \in \mathbb{N}_0$ for all $\ell \in \{1, \dots, L\}$, so $N = Ln$. Evaluating $\tilde{\Lambda} \in \mathbb{C}^{N \times N}$ requires $O(L^2(n \log n + dn))$ computations and $O(L^2n)$ storage. Having evaluated $\tilde{\Lambda}$, computing $\tilde{\mathbf{K}}\mathbf{y} = \sqrt{\tilde{\Lambda}}\tilde{\mathbf{V}}\mathbf{y}$ for any $\mathbf{y} \in \mathbb{R}^N$ requires $O(Ln \log n + L^2n)$ computations. Having evaluated $\tilde{\Lambda}$, evaluating $|\tilde{\mathbf{K}}| = |\tilde{\Lambda}|$ and $\tilde{\Lambda}^{-1}$ using [Algorithm 1](#) requires $O(L^3n)$ computations and $O(L^2n)$ storage. Having stored $\tilde{\Lambda}^{-1}$, evaluating $\tilde{\mathbf{K}}^{-1}\mathbf{y} = \sqrt{\tilde{\Lambda}^{-1}}\tilde{\mathbf{V}}\mathbf{y}$ for any $\mathbf{y} \in \mathbb{R}^N$ requires $O(Ln \log n + L^2n)$ computations.

For fast multitask Bayesian cubature, let us define $\Pi := \left(\sqrt{n_\ell n_{\ell'}} (\tilde{\Lambda}^{-1})_{N_{\ell-1}, N_{\ell'-1}} \right)_{\ell, \ell'=1}^L \in \mathbb{R}^{L \times L}$ and $\mathbf{H} := \left(\sqrt{n_\ell} (\tilde{\Lambda}^{-1})_{N_{\ell-1}, k_{n_\ell}} \right)_{\ell=1, k=0}^{L, N/n_L-1} \in \mathbb{C}^{L \times N/n_L}$ where $N_0 = 0$ and $N_\ell = n_1 + \dots + n_\ell$, and we still assume $n_1 \geq \dots \geq n_L$.

Theorem 2.7 (MTGP optimal prior mean constants). Under [Condition 2.3](#), the optimal NMLL and GCV prior mean constants in [\(12\)](#) respectively satisfy

$$\Pi \tau_{\text{NMLL}} = \tilde{\mathbf{E}}\tilde{\mathbf{K}}^{-1}\mathbf{y} \quad \text{and} \quad (\mathbf{H}\mathbf{H}^\top)\tau_{\text{GCV}} = \tilde{\mathbf{E}}\tilde{\mathbf{K}}^{-2}\mathbf{y}.$$

For fast multitask Bayesian cubature, we need the following condition analogous to [Condition 2.2](#).

Algorithm 1 Inverse and determinant of $\widetilde{\Lambda}$

Require: $\widetilde{\Lambda}$ diagonal block matrix with $m_1 \geq \dots \geq m_L$.

$D \leftarrow \widetilde{\Lambda}_{11}$ $\triangleright A 2^{m_1} \times 2^{m_1}$ diagonal matrix.
 $A \leftarrow D^{-1}$ $\triangleright A 2^{m_1} \times 2^{m_1}$ diagonal matrix. Costs $O(2^{m_1})$.
 $\varrho \leftarrow |D|$ $\triangleright A$ scalar. Costs $O(2^{m_1})$.
 $\ell \leftarrow 2$
while $\ell \leq L$ **do**
 $D \leftarrow \widetilde{\Lambda}_{\ell\ell}$ $\triangleright A 2^{m_\ell} \times 2^{m_\ell}$ diagonal matrix.
 $B \leftarrow \widetilde{\Lambda}_{:(\ell-1),\ell}$ $\triangleright A \sum_{\ell'=1}^{\ell-1} 2^{m_{\ell'}-m_\ell} \times 1$ block matrix with $2^{m_\ell} \times 2^{m_\ell}$ diagonal blocks.
 $L \leftarrow AB$ $\triangleright A \sum_{\ell'=1}^{\ell-1} 2^{m_{\ell'}-m_\ell} \times 1$ block matrix with $2^{m_\ell} \times 2^{m_\ell}$ diagonal blocks. Costs $O([\sum_{\ell'=1}^{\ell-1} 2^{m_{\ell'}-m_{\ell-1}}][\sum_{\ell'=1}^{\ell-1} 2^{m_{\ell'}}])$.
 $F \leftarrow B^T L$ $\triangleright A 2^{m_\ell} \times 2^{m_\ell}$ diagonal matrix. Costs $O(\sum_{\ell'=1}^{\ell-1} 2^{m_{\ell'}})$.
 $S \leftarrow D - F$ $\triangleright A 2^{m_\ell} \times 2^{m_\ell}$ diagonal matrix (the Schur complement). Costs 2^{m_ℓ} .
 $\varrho \leftarrow \varrho |S|$ $\triangleright A$ scalar. Costs $O(2^{m_\ell})$. Equivalent to $|\Lambda_{:\ell,:\ell}|$.
 $G \leftarrow S^{-1}$ $\triangleright A 2^{m_\ell} \times 2^{m_\ell}$ diagonal matrix. Costs $O(2^{m_\ell})$.
 $H \leftarrow LG$ $\triangleright A \sum_{\ell'=1}^{\ell-1} 2^{m_{\ell'}-m_\ell} \times 1$ block matrix with $2^{m_\ell} \times 2^{m_\ell}$ diagonal blocks. Costs $O(\sum_{\ell'=1}^{\ell-1} 2^{m_{\ell'}})$.
 $J \leftarrow H L^T$ $\triangleright A \sum_{\ell'=1}^{\ell-1} 2^{m_{\ell'}-m_\ell} \times \sum_{\ell'=1}^{\ell-1} 2^{m_{\ell'}-m_\ell}$ block matrix with $2^{m_\ell} \times 2^{m_\ell}$ diagonal blocks. Costs $O([\sum_{\ell'=1}^{\ell-1} 2^{m_{\ell'}-m_\ell}][\sum_{\ell'=1}^{\ell-1} 2^{m_{\ell'}}])$.
 $M \leftarrow A + J$ $\triangleright A \sum_{\ell'=1}^{\ell-1} 2^{m_{\ell'}-m_\ell} \times \sum_{\ell'=1}^{\ell-1} 2^{m_{\ell'}-m_\ell}$ block matrix with $2^{m_\ell} \times 2^{m_\ell}$ diagonal blocks. Costs $O([\sum_{\ell'=1}^{\ell-1} 2^{m_{\ell'}-m_\ell}][\sum_{\ell'=1}^{\ell-1} 2^{m_{\ell'}}])$.
 $A \leftarrow \begin{pmatrix} M & -H \\ -H^T & G \end{pmatrix}$ $\triangleright A \sum_{\ell'=1}^{\ell} 2^{m_{\ell'}-m_\ell} \times \sum_{\ell'=1}^{\ell} 2^{m_{\ell'}-m_\ell}$ block matrix with $2^{m_\ell} \times 2^{m_\ell}$ diagonal blocks. Equivalent to $\widetilde{\Lambda}_{:\ell,:\ell}^{-1}$.
 $\ell \leftarrow \ell + 1$
 $\widetilde{\Lambda}^{-1} \leftarrow A$ $\triangleright A \sum_{\ell=1}^L 2^{m_\ell-m_L} \times \sum_{\ell=1}^L 2^{m_\ell-m_L}$ block matrix with $2^{m_L} \times 2^{m_L}$ diagonal blocks.
 $|\widetilde{\Lambda}| \leftarrow \varrho$ $\triangleright A$ scalar.
return $\widetilde{\Lambda}^{-1}, |\widetilde{\Lambda}|$

Condition 2.4 (Fast Bayesian cubature). For some $\gamma \in \mathbb{R}_+$, $\int_{[0,1]^d} Q(\mathbf{x}, \mathbf{x}') d\mathbf{x}' = \gamma$ holds for all $\mathbf{x} \in [0, 1]^d$.

Theorem 2.8. Under [Condition 2.3](#) and [Condition 2.4](#), $\Sigma = \gamma R - \gamma^2 R \Pi R \in \mathbb{R}^{L \times L}$ from [\(13\)](#).

Remark 2.2 (Fast derivative informed GPs). [Sorokin et al. \(2025b\)](#) explored incorporating derivative information into fast GPs, mostly relying on the fact that derivatives of certain SI kernels are also SI. Their work only considered the equal sample size case, $n_1 = \dots = n_L$, i.e., L different derivative orders were observed for each collocation point. The structures and algorithms they derived form the basis of what we generalize in this work.

3. Numerical Experiments

3.1. Scope of Configurations

Our experiments use the FastGPs package (<https://alegresor.github.io/fastgps/>) ([Sorokin et al., 2025b](#); [Sorokin, 2025a](#)) with the linked documentation containing a demo reproducing numerical experiments from this paper. FastGPs uses the quasi-Monte Carlo package

QMCPy (<https://qmsoftware.github.io/QMCSsoftware/>) (Choi et al., 2022b,a) for generating low-discrepancy lattices and digital sequences. We will compare across the following three methods:

Cholesky SE The FastGPs implementation of standard MTGPs in Section 2.3 using the spatial squared exponential kernel in (1) with the full Cholesky decomposition.

CG SE (GPyTorch) The GPyTorch (Gardner et al., 2018a) implementation of standard MTGPs using the spatial squared exponential kernel in (1) and the (preconditioned) conjugate gradient (CG) method for solving the Gram matrix systems. This requires an approximation for the log determinant and its gradient using the Lanczos tridiagonalization algorithm and stochastic trace estimation respectively.

Fast DSI (ours) The FastGPs implementation of the fast MTGPs presented in this article using digital sequences and matching digitally-shift-invariant (DSI) kernels, i.e., using the DSI-DSEQ variant in Condition 2.3.

The problems we consider are detailed in the following subsections. Table 2 gives parameters for each problem. Implementations of these problems can be found in the Virtual Library of Simulation Experiments (VLSE) (Surjanovic and Bingham, 2013), QMCPy (Choi et al., 2022b,a), or the language-agnostic UM-Bridge framework for uncertainty quantification and containerized model distribution (Seelinger et al., 2023).

For each problem, we optimize the negative marginal log-likelihood (NMLL) in (11) using the resilient backpropagation algorithm (Rprop) (Riedmiller and Braun, 1993) in PyTorch (Paszke et al., 2019). We fix the noise variance to $\xi = 10^{-4}$ for both Cholesky SE and CG SE (GPyTorch), while for our Fast MTGPs we use a noise of around 4.4×10^{-16} . All computations were run on an M3 MacBook Pro in double precision.

We do not consider the lattice shift-invariant (SI-LAT) variant in Condition 2.3, nor do we consider minimizing the generalized cross validation (GCV) loss in (11). Some preliminary experiments suggest the periodicity requirement for the SI-LAT variant significantly hurts performance. Coupling the proposed method with periodizing transforms and comparing the NMLL versus GCV loss are valuable avenues for future work.

We will start by fitting a fast MTGP to the Rosenbrock function in Section 3.2 with large N . Then we will run a range of n values for the Ackley (Section 3.3), Borehole (Section 3.4), Elliptic PDE (Section 3.5), and Cookie (Section 3.6) problems. Section 3.7 will summarize experimental results.

3.2. Rosenbrock

Let us begin with a simple $d = 2$ Rosenbrock example with $L = 3$ as considered by Wackers et al. (2023) with the low fidelity model from Rumpfkeil and Beran (2020):

$$\begin{aligned} f(1, \mathbf{x}) &= (f(3, \mathbf{x}) - 4 - 0.5x_1 - 0.5x_2)/(10 + 0.25x_1 + 0.25x_2), \\ f(2, \mathbf{x}) &= 50(x_2 - x_1^2)^2 + (-2 - x_1)^2 - 80 - 0.25x_1x_2, \\ f(3, \mathbf{x}) &= 100(x_2 - x_1^2)^2 + (1 - x_1)^2. \end{aligned}$$

Problem	d	L	$\mathbf{n} \in$	Section
Rosenbrock	2	3	$\{\{2^{15}, 2^{14}, \dots, 2^{13}\}\}$	3.2
Ackley	4	2	$\times_{\ell=1}^L \{2^5, 2^6, \dots, 2^{15}\}$	3.3
Borehole	8	2	$\times_{\ell=1}^L \{2^5, 2^6, \dots, 2^{15}\}$	3.4
Elliptic PDE	16	3	$\times_{\ell=1}^L \{2^5, 2^7, 2^9, 2^{11}, 2^{13}\}$	3.5
Cookie	8	4	$\times_{\ell=1}^L \{2^5, 2^7, 2^9, 2^{11}, 2^{13}\}$	3.6

Table 2: Problem parameters including the dimension d , the number of tasks L , and sample sizes \mathbf{n} considered

Figure 4 visualizes our fast MTGP DSI-DSEQ variant fit to $N = 57344$ points. Equivalent fitting for standard MTGPs would require large scale computing resources and be infeasible on a personal laptop. Fitting our fast MTGP for almost 200 NMLL optimization steps took less than 15 seconds on a laptop with each optimization step requiring less than a tenth of a second. Moreover, the multitask DSI kernels were accurate enough to recover solutions at each fidelity to less than 1% L_2 relative error

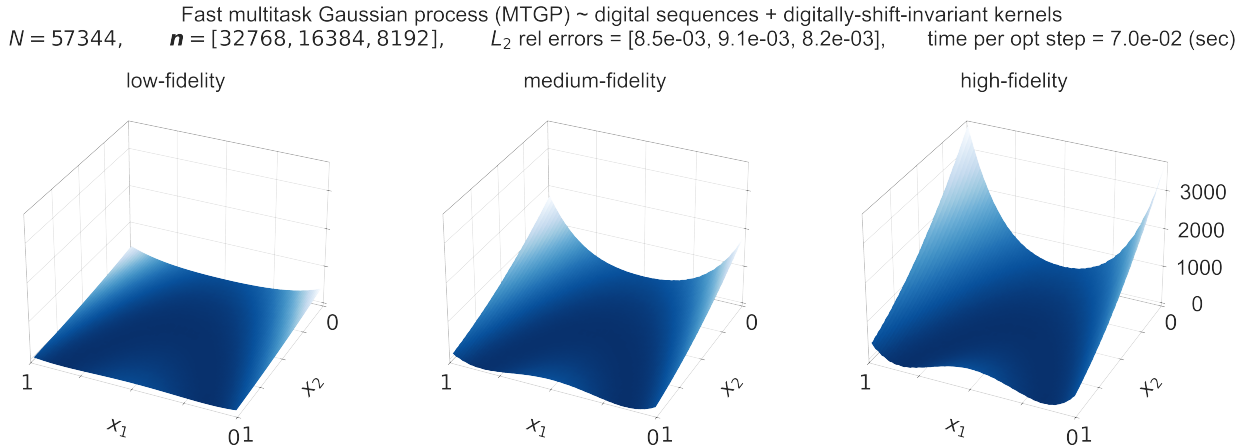


Figure 4: Posterior mean estimates of a fast MTGP fit to the multifidelity Rosenbrock function.

3.3. Ackley

The Ackley function is

$$f(\mathbf{x}) = g(\Phi^{-1}(\mathbf{x})), \quad \Phi^{-1}(\mathbf{x}) = 65.536\mathbf{x} - 32.768,$$

$$g(\mathbf{t}) = -20 \exp\left(-0.2 \sqrt{\frac{1}{d} \sum_{j=1}^d t_j^2}\right) - \exp\left(\frac{1}{d} \sum_{j=1}^d \cos(ct_j)\right) + a + \exp(1).$$

The low-fidelity $\ell = 1$ task sets $c = 0$ while the high-fidelity $\ell = 2$ task sets $c = 2\pi$. For $\mathbf{X} \sim \mathcal{U}[0, 1]^d$ we have $\mathbf{T} = \Phi^{-1}(\mathbf{X}) \sim \mathcal{U}[-32.768, 32.768]^d$. We will consider the $d = 4$ case.

3.4. Borehole

The Borehole function models water flow through a borehole with

$$f(\mathbf{x}) = g(\Phi^{-1}(\mathbf{x})), \quad g(\mathbf{t}) = \frac{c_1 \pi T_u (H_u - H_l)}{\log(r_i/r_w) \left(c_2 + \frac{2L_b T_u}{\log(r_i/r_w) r_w^2 K_w} + \frac{T_u}{T_l} \right)}$$

where Φ^{-1} applies the inverse CDF transform so that for $\mathbf{X} \sim \mathcal{U}[0, 1]^d$ we have that $(r_w, r_i, T_u, H_u, T_l, H_l, L_b, K_w) = \Phi^{-1}(\mathbf{X})$ has independent marginals with parameters given in [Table 3](#). Following ([Xiong et al., 2013](#)), the low-fidelity $\ell = 1$ task sets $(c_1, c_2) = (2, 1)$ while the high-fidelity $\ell = 1$ task sets $(c_1, c_2) = (5, 3/2)$.

parameter	description
$r_w \sim \mathcal{N}(0.1, 0.0161812^2)$	radius of borehole (m)
$r_i \sim \text{lognormal}(7.71, 1.0056^2)$	radius of influence (m)
$T_u \sim \mathcal{U}[63070, 115600]$	transmissivity of upper aquifer (m ² /yr)
$H_u \sim \mathcal{U}[990, 1110]$	potentiometric head of upper aquifer (m)
$T_l \sim \mathcal{U}[63.1, 116]$	transmissivity of lower aquifer (m ² /yr)
$H_l \sim \mathcal{U}[700, 820]$	potentiometric head of lower aquifer (m)
$L_b \sim \mathcal{U}[1120, 1680]$	length of borehole (m)
$K_w \sim \mathcal{U}[9855, 12045]$	hydraulic conductivity of borehole (m/yr)

Table 3: Parameters of the borehole function. $\text{lognormal}(\mu, \sigma^2)$ is the lognormal distribution of a variable such that the natural logarithm of the variable has a $\mathcal{N}(\mu, \sigma^2)$ distribution.

3.5. Elliptic PDE

Let us consider the one-dimensional elliptic PDE $-\nabla(e^{a(u,\mathbf{x})})\nabla F(u, \mathbf{x}) = g(u)$ with $u \in [0, 1]$ and boundary conditions $F(0, \mathbf{x}) = F(1, \mathbf{x}) = 0$ for all $\mathbf{x} \in [0, 1]^d$. The forcing term g is set to the constant $g(u) = 1$ for all $u \in [0, 1]$. We will generate $a(u, \mathbf{x}) = \sum_{j=1}^d \Phi^{-1}(x_j) \sin(\pi k u)/j$ in $d = 16$ dimensions and Φ the CDF of the standard normal so $\Phi^{-1}(X_j) \sim \mathcal{N}(0, 1)$. Let us denote by F_ℓ the task ℓ numerical PDE solution using a finite difference method with $2^{1+\ell} + 1$ evenly spaced mesh points $(k/2^{1+\ell})_{k=0}^{2^{1+\ell}}$. We will take the discretized solution to be $f(\ell, \mathbf{x}) = \max_u F_\ell(u, \mathbf{x})$ and use $L = 3$ tasks. For each query of $f(\ell, \cdot)$ we need to solve a tridiagonal linear system, which can be done with linear complexity.

3.6. Cookies in the Oven

This problem simulates baking cookies subject to uncertainty in the conductivity coefficients in $d = 8$ circular subdomains (the cookies). We use the implementation in UM-Bridge ([Seelinger et al., 2023](#)), an uncertainty quantification framework which provides containerized language-agnostic models. Under the hood, the UM-Bridge implementation calls the finite element solver from FEniCS ([Baratta et al., 2023](#)) with quadrilateral meshes and the stationary equation which results in an elliptic type PDE, see ([Bäck et al., 2010](#); [Ballani and Grasedyck, 2015](#); [Kressner and Tobler, 2011](#)) for details. For each of the 4 tasks we use 100ℓ mesh points for the finite

element solver in each dimension, e.g., for our two-dimensional physical domain the highest-fidelity $\ell = 4$ mesh has 400^2 nodes. We again take $f(\mathbf{x}) = g(\Phi^{-1}(\mathbf{X}))$ where g is the numerical solver accessed through UM-Bridge and $\Phi^{-1}(\mathbf{x}) = 0.79\mathbf{x} - 0.99$ so for $\mathbf{X} \sim \mathcal{U}[0, 1]^d$ we have $\Phi^{-1}(\mathbf{X}) \sim \mathcal{U}[-0.99, -0.2]$.

3.7. Benchmark Results

For the Ackley, borehole, elliptic PDE, and cookie problems we ran experiments across a wide range of n values in grids specified in Table 2. For each n , we ran 5 independent trails and compare the median time per optimization step against both the median L_2 relative errors and Bayesian cubature errors. L_2 relative errors are approximated using 2048 LD test points. For the CG SE variant, Bayesian cubature is not directly supported in GPyTorch, so we use the 2048 LD test points to compute a QMC estimate of the Bayesian cubature mean. Due to memory and time constraints, we only run Cholesky SE when $N \leq 2048$, and we only ran CG SE (GPyTorch) when $N \leq 4096$. All Bayesian cubature errors are computed for the last task $\ell = L$, the highest-fidelity model.

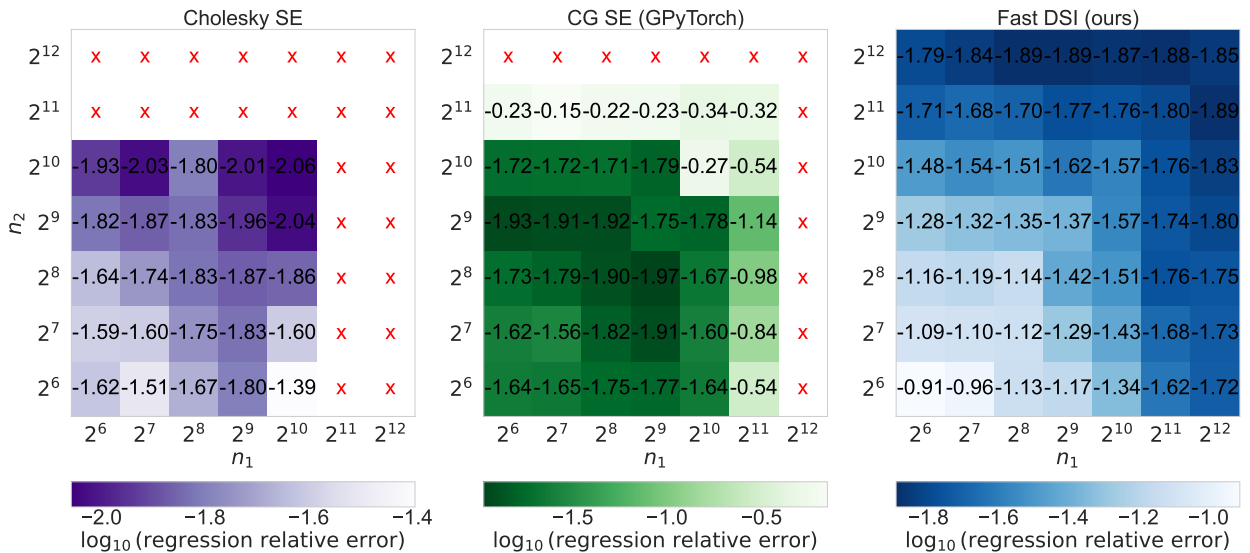


Figure 5: Regression L_2 relative errors for the borehole problem.

Figure 5 visualizes the errors for the borehole problem across the range of tested n values. For the visualized n , Cholesky SE was able to achieve the lowest errors despite not being able to support the larger n values accommodated by CG SE or even larger values for our fast MTGP. We found the error for the GPyTorch implementation generally decreases with n , but then spikes when n becomes large. For example, we found errors of around $1e-1.8$ at $\mathbf{n} = (2^{10}, 2^9)^\top$ and $\mathbf{n} = (2^9, 2^{10})^\top$, but for $\mathbf{n} = (2^{10}, 2^{10})^\top$ or greater, the error spiked to $1e-0.3$. The poor performance of GPyTorch for large n was consistent across all experiments and may be attributed to poor NMLL optimization performance or an insufficient number of optimization iterations.

When pushing fast MTGPs to larger n , we observed the lowest errors achieved across all three methods. This finding is consistent across all problems where, for a fixed n , the SE kernel generally gives slightly better performance than the DSI kernels, but the scalability of our fast DSI-DSEQ methods allows for accommodating large enough n to achieve better errors in less optimization time.

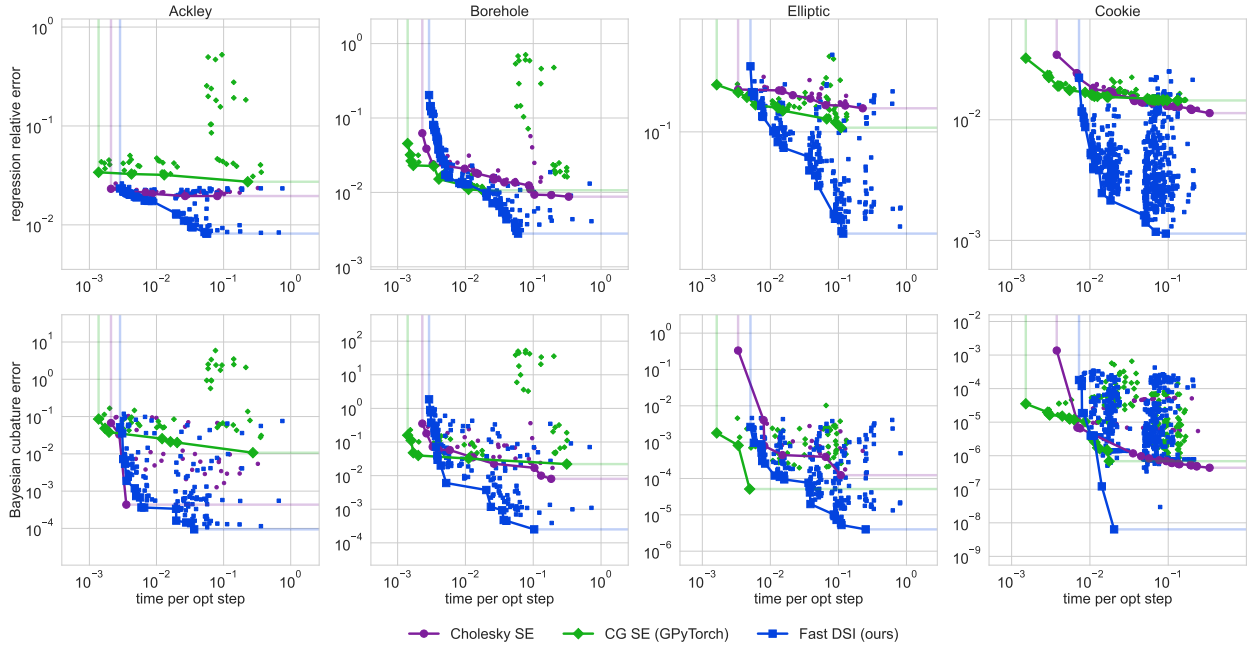


Figure 6: Pareto frontiers for L_2 relative regression errors and Bayesian cubature errors versus time per optimization step.

Figure 6 compares the time per optimization step against both the L_2 relative regression errors and the absolute Bayesian cubature errors. The approximate Pareto frontier is plotted along which improved errors can only be observed by increasing the time-per-optimization step. Here we clearly see the advantage of fast MTGPs compared to standard methods. For many cases we found an order of magnitude improvement for our fast GPs. For instance, in the cookie problem we were able to achieve L_2 relative regression errors of nearly 10^{-3} in the same amount of time-per-step it takes the Cholesky SE and CG SE methods to achieve errors of only 10^{-2} . Similar regression error savings were observed across the other benchmark problems as well.

For Bayesian cubature, our fast MTGP methods again significantly outperform the other two baseline methods. For example, on the borehole and Elliptic PDE problems, the fast MTGP method had cubature errors around an order of magnitude better than the full Cholesky method at the same time-per-step. Even more impressive is the nearly 100 times cubature error reduction for the cookie problem at a fraction of the cost. Specifically, the fast MTGP method achieved errors less than 10^{-8} while the Cholesky SE and CG SE methods were only able to achieve errors like 10^{-6} after investing an order of magnitude more compute per step.

4. Conclusions and Future Work

This article generalized fast Gaussian process (GP) regression using low-discrepancy (LD) sequences and matching (digitally-)shift invariant kernels to the multitask GP (MTGP) setting. Our fast MTGP methods accommodate lattice and digital sequences with different shifts on each level and different sample sizes on each level. We developed a scalable open-source implementation in the FastGP Python package and ran numerous benchmark problems to demonstrate the performance of the proposed methods.

We have identified the following items as valuable future work.

Extended testing In this article we have only tested fast MTGPs with the DSI-DSEQ variant fit by optimizing the negative marginal log-likelihood (NMLL) loss. Experiments should be done to compare against the SI-LAT variant in [Condition 2.3](#) and the GCV loss in (11). Tests should also be conducted to evaluate the performance of the optimal multitask Bayesian cubature weights discussed in [Section Appendix A](#).

Other multitask structured kernel interpolation methods One may build off the methods in this work to extend other structured kernel interpolation methods to the multitask setting. In the single task setting, pairing grid points with (stationary) product kernels has shown strong performance. Pairing Kronecker sequences ([Drmotá and Tichý, 2006](#), Section 1.4) with shift-invariant kernels will also include nice structure into single-task Gram matrices which could potentially be extended to the multitask setting as well.

Acknowledgements

FH, PR, and AS acknowledge that this work is supported by National Science Foundation DMS Grant No. 2316011.

AS is partially supported by DARPA The Right Space HR0011-25-9-0031.

AS acknowledges that this material is based upon work supported by the U.S. Department of Energy, Office of Science, Office of Work-force Development for Teachers and Scientists, Office of Science Graduate Student Research (SCGSR) program. The SCGSR program is administered by the Oak Ridge Institute for Science and Education for the DOE under contract number DE-SC0014664.

PR and AS acknowledge that this work was supported by the Laboratory Directed Research and Development (LDRD) program and the Advanced Simulation and Computing, Verification and Validation (ASC V&V) program at Sandia National Laboratories.

PR and AS acknowledge that this article has been co-authored by employees of National Technology and Engineering Solutions of Sandia, LLC under Contract No. DE-NA0003525 with the U.S. Department of Energy (DOE). The employees co-own right, title and interest in and to the article and are responsible for its contents. The United States Government retains and the publisher, by accepting the article for publication, acknowledges that the United States Government retains a non-exclusive, paid-up, irrevocable, world-wide license to publish or reproduce the published form of this article or allow others to do so, for United States Government purposes.

The DOE will provide public access to these results of federally sponsored research in accordance with the DOE Public Access Plan available at <https://www.energy.gov/downloads/doe-public-access-plan>.

References

- Bäck, J., Nobile, F., Tamellini, L., Tempone, R., 2010. Stochastic spectral Galerkin and collocation methods for PDEs with random coefficients: a numerical comparison, in: Spectral and High Order Methods for Partial Differential Equations: Selected papers from the ICOSAHOM'09 conference, June 22–26, Trondheim, Norway, Springer. pp. 43–62.
- Ballani, J., Grasedyck, L., 2015. Hierarchical tensor approximation of output quantities of parameter-dependent PDEs. *SIAM/ASA Journal on Uncertainty Quantification* 3, 852–872.
- Banerjee, S., Gelfand, A.E., Sirmans, C.F., 2003. Directional rates of change under spatial process models. *Journal of the American Statistical Association* 98, 946–954.
- Baratta, I.A., Dean, J.P., Dokken, J.S., Habera, M., Hale, J.S., Richardson, C.N., Rognes, M.E., Scroggs, M.W., Sime, N., Wells, G.N., 2023. DOLFINx: the next generation FEniCS problem solving environment. preprint. doi:[10.5281/zenodo.10447666](https://doi.org/10.5281/zenodo.10447666).
- Bonilla, E.V., Chai, K.M.A., Williams, C.K.I., 2007. Multi-task Gaussian process prediction, in: Platt, J.C., Koller, D., Singer, Y., Roweis, S.T. (Eds.), *Advances in Neural Information Processing Systems*, Curran Associates, Inc.. pp. 153–160. URL: <https://proceedings.neurips.cc/paper/2007/hash/66368270ffd51418ec58bd793f2d9b1b-Abstract.html>.
- Charlier, B., Feydy, J., Glaunès, J.A., Collin, F.D., Durif, G., 2021. Kernel operations on the GPU, with autodiff, without memory overflows. *Journal of Machine Learning Research* 22, 1–6. URL: <http://jmlr.org/papers/v22/20-275.html>.
- Choi, S.C.T., Ding, Y., Hickernell, F.J., Rathinavel, J., Sorokin, A.G., 2022a. Challenges in developing great quasi-Monte Carlo software, in: Hinrichs, A., Kritzer, P., Pillichshammer, F. (Eds.), *Monte Carlo and Quasi-Monte Carlo Methods 2022*, Springer. pp. 209–222.
- Choi, S.C.T., Hickernell, F.J., Rathinavel, J., McCourt, M.J., Sorokin, A.G., 2022b. Quasi-Monte Carlo software, in: Keller, A. (Ed.), *Monte Carlo and Quasi-Monte Carlo Methods 2020*, Springer International Publishing, Cham. pp. 23–47.
- Cooley, J.W., Tukey, J.W., 1965. An algorithm for the machine calculation of complex Fourier series. *Mathematics of Computation* 19, 297–301.
- Cools, R., Kuo, F.Y., Nuyens, D., Sloan, I.H., 2020. Lattice algorithms for multivariate approximation in periodic spaces with general weight parameters, in: *75 years of mathematics of computation*, pp. 93–113. doi:[10.1090/conm/754/15150](https://doi.org/10.1090/conm/754/15150).

- Cools, R., Kuo, F.Y., Nuyens, D., Sloan, I.H., 2021. Fast component-by-component construction of lattice algorithms for multivariate approximation with POD and SPOD weights. *Mathematics of Computation* 90, 787–812.
- van der Corput, J.G., 1935. Verteilungsfunktionen. I. *Proc. Akad. Wet. Amsterdam* 38, 813–821.
- Craven, P., Wahba, G., 1978. Smoothing noisy data with spline functions: estimating the correct degree of smoothing by the method of generalized cross-validation. *Numerische mathematik* 31, 377–403.
- Dick, J., Kritzer, P., Pillichshammer, F., 2022. *Lattice rules*. Springer.
- Dick, J., Pillichshammer, F., 2005. Multivariate integration in weighted Hilbert spaces based on Walsh functions and weighted Sobolev spaces. *Journal of Complexity* 21, 149–195.
- Dick, J., Pillichshammer, F., 2010. *Digital nets and sequences: discrepancy theory and quasi-Monte Carlo integration*. Cambridge University Press.
- Drumota, M., Tichy, R.F., 2006. *Sequences, discrepancies and applications*. Springer.
- Duvenaud, D., 2014. *Automatic model construction with Gaussian processes*. Ph.D. thesis. Apollo - University of Cambridge Repository. URL: <https://www.repository.cam.ac.uk/handle/1810/247281>, doi:10.17863/CAM.14087.
- Eriksson, D., Dong, K., Lee, E.H., Bindel, D., Wilson, A.G., 2018. Scaling Gaussian process regression with derivatives, in: Bengio, S., Wallach, H.M., Larochelle, H., Grauman, K., Cesa-Bianchi, N., Garnett, R. (Eds.), *Advances in Neural Information Processing Systems*, Curran Associates, Inc.. pp. 6868–6878. URL: <https://proceedings.neurips.cc/paper/2018/hash/c2f32522a84d5e6357e6abac087f1b0b-Abstract.html>.
- Fasshauer, G.E., 2007. *Meshfree approximation methods with MATLAB*. volume 6. World Scientific.
- Fino, Algazi, 1976. Unified matrix treatment of the fast Walsh–Hadamard transform. *IEEE Transactions on Computers* 100, 1142–1146.
- Gardner, J.R., Pleiss, G., Weinberger, K.Q., Bindel, D., Wilson, A.G., 2018a. GP-Torch: blackbox matrix-matrix Gaussian process inference with GPU acceleration, in: Bengio, S., Wallach, H.M., Larochelle, H., Grauman, K., Cesa-Bianchi, N., Garnett, R. (Eds.), *Advances in Neural Information Processing Systems*, Curran Associates, Inc.. pp. 7587–7597. URL: <https://proceedings.neurips.cc/paper/2018/hash/27e8e17134dd7083b050476733207ea1-Abstract.html>.
- Gardner, J.R., Pleiss, G., Wu, R., Weinberger, K.Q., Wilson, A.G., 2018b. Product kernel interpolation for scalable Gaussian processes, in: Storkey, A.J., Pérez-Cruz, F. (Eds.), *International Conference on Artificial Intelligence and Statistics, AISTATS 2018*, 9-11 April 2018, Playa Blanca, Lanzarote, Canary Islands, Spain, PMLR. pp. 1407–1416. URL: <http://proceedings.mlr.press/v84/gardner18a.html>.

- Giles, M.B., 2008. Multilevel Monte Carlo path simulation. *Operations research* 56, 607–617.
- Giles, M.B., 2015. Multilevel Monte Carlo methods. *Acta Numerica* 24, 259–328. doi:[10.1017/S096249291500001X](https://doi.org/10.1017/S096249291500001X).
- Giles, M.B., Waterhouse, B.J., 2009. Multilevel quasi-Monte Carlo path simulation. *Advanced Financial Modelling, Radon Series on Computational and Applied Mathematics* 8, 165–181.
- Golub, G.H., Heath, M., Wahba, G., 1979. Generalized cross-validation as a method for choosing a good ridge parameter. *Technometrics* 21, 215–223.
- Kaarnioja, V., Kazashi, Y., Kuo, F.Y., Nobile, F., Sloan, I.H., 2022. Fast approximation by periodic kernel-based lattice-point interpolation with application in uncertainty quantification. *Numerische Mathematik*, 1–45.
- Kaarnioja, V., Kuo, F.Y., Sloan, I.H., 2023. Lattice-based kernel approximation and serendipitous weights for parametric PDEs in very high dimensions. *ArXiv preprint abs/2303.17755*. URL: <https://arxiv.org/abs/2303.17755>.
- Kressner, D., Tobler, C., 2011. Low-rank tensor Krylov subspace methods for parametrized linear systems. *SIAM Journal on Matrix Analysis and Applications* 32, 1288–1316.
- Kuo, F.Y., Sloan, I.H., Woźniakowski, H., 2004. Lattice rules for multivariate approximation in the worst case setting, in: Niederreiter, H., Talay, D. (Eds.), *Monte Carlo and Quasi-Monte Carlo Methods 2004*. Springer, pp. 289–330.
- Owhadi, H., Scovel, C., 2019. *Operator-adapted wavelets, fast solvers, and numerical homogenization: from a game theoretic approach to numerical approximation and algorithm design*. volume 35. Cambridge University Press.
- Padidar, M., Zhu, X., Huang, L., Gardner, J., Bindel, D., 2021. Scaling Gaussian processes with derivative information using variational inference, in: Ranzato, M., Beygelzimer, A., Dauphin, Y., Liang, P.S., Vaughan, J.W. (Eds.), *Advances in Neural Information Processing Systems*, Curran Associates, Inc.. pp. 6442–6453. URL: <https://proceedings.neurips.cc/paper/2021/hash/32bbf7b2bc4ed14eb1e9c2580056a989-Abstract.html>.
- Paszke, A., Gross, S., Massa, F., Lerer, A., Bradbury, J., Chanan, G., Killeen, T., Lin, Z., Gimelshein, N., Antiga, L., Desmaison, A., Köpf, A., Yang, E., DeVito, Z., Raison, M., Tejani, A., Chilamkurthy, S., Steiner, B., Fang, L., Bai, J., Chintala, S., 2019. PyTorch: an imperative style, high-performance deep learning library, in: Wallach, H.M., Larochelle, H., Beygelzimer, A., d’Alché-Buc, F., Fox, E.B., Garnett, R. (Eds.), *Advances in Neural Information Processing Systems*, Curran Associates, Inc.. pp. 8024–8035. URL: <https://proceedings.neurips.cc/paper/2019/hash/bdbca288fee7f92f2bfa9f7012727740-Abstract.html>.
- Rasmussen, C.E., Williams, C.K.I., 2006. *Gaussian processes for machine learning*. MIT Press, Cambridge, Massachusetts. URL: <http://www.gaussianprocess.org/gpml/>.

- Rathinavel, J., 2019. Fast automatic Bayesian cubature using matching kernels and designs. Ph.D. thesis. Illinois Institute of Technology.
- Rathinavel, J., Hickernell, F.J., 2019. Fast automatic Bayesian cubature using lattice sampling. *Statistics and Computing* 29, 1215–1229. URL: <http://dx.doi.org/10.1007/s11222-019-09895-9>, doi:10.1007/s11222-019-09895-9.
- Rathinavel, J., Hickernell, F.J., 2022. Fast automatic Bayesian cubature using Sobol’ sampling, in: *Advances in Modeling and Simulation: Festschrift for Pierre L’Ecuyer*. Springer, pp. 301–318.
- Riedmiller, M., Braun, H., 1993. A direct adaptive method for faster backpropagation learning: the RPROP algorithm, in: *IEEE international conference on neural networks*, IEEE. pp. 586–591.
- Rumpfkeil, M.P., Beran, P.S., 2020. Multi-fidelity, gradient-enhanced, and locally optimized sparse polynomial chaos and kriging surrogate models applied to benchmark problems, in: *AIAA Scitech 2020 Forum*, p. 0677.
- Saatçi, Y., 2012. Scalable inference for structured Gaussian process models. Ph.D. thesis. Citeseer.
- Seelinger, L., Cheng-Seelinger, V., Davis, A., Parno, M., Reinartz, A., 2023. UM-Bridge: uncertainty quantification and modeling bridge. *Journal of Open Source Software* 8, 4748.
- Sloan, I.H., Woźniakowski, H., 2001. Tractability of multivariate integration for weighted Korobov classes. *Journal of Complexity* 17, 697–721.
- Solak, E., Murray-Smith, R., Leithead, W.E., Leith, D.J., Rasmussen, C.E., 2002. Derivative observations in Gaussian process models of dynamic systems, in: Becker, S., Thrun, S., Obermayer, K. (Eds.), *Advances in Neural Information Processing Systems*, MIT Press. pp. 1033–1040. URL: <https://proceedings.neurips.cc/paper/2002/hash/5b8e4fd39d9786228649a8a8bec4e008-Abstract.html>.
- Sorokin, A.G., 2025a. Algorithms and scientific software for quasi-Monte Carlo, fast Gaussian process regression, and scientific machine learning. Ph.D. thesis. Illinois Institute of Technology. URL: <https://arxiv.org/abs/2511.21915>.
- Sorokin, A.G., 2025b. QMCPy: a Python software for randomized low-discrepancy sequences, quasi-Monte Carlo, and fast kernel methods. *ArXiv preprint abs/2502.14256*. URL: <https://arxiv.org/abs/2502.14256>.
- Sorokin, A.G., Pachaliev, A., O’Malley, D., Hyman, J.M., Hickernell, F.J., Hengartner, N.W., 2024. Computationally efficient and error aware surrogate construction for numerical solutions of subsurface flow through porous media. *Advances in Water Resources* 193, 104836. URL: <https://www.sciencedirect.com/science/article/pii/S0309170824002239>, doi:10.1016/j.advwatres.2024.104836.

- Sorokin, A.G., Robbe, P., Geraci, G., Eldred, M.S., Hickernell, F.J., 2025a. Fast Bayesian multilevel quasi-Monte Carlo. ArXiv preprint abs/2510.24604. URL: <https://arxiv.org/abs/2510.24604>.
- Sorokin, A.G., Robbe, P., Hickernell, F.J., 2025b. Fast Gaussian process regression for high dimensional functions with derivative information, in: Kanagawa, M., Cockayne, J., Gessner, A., Hennig, P. (Eds.), Proceedings of the First International Conference on Probabilistic Numerics, PMLR. pp. 35–49. URL: <https://proceedings.mlr.press/v271/sorokin25a.html>.
- Surjanovic, S., Bingham, D., 2013. Virtual library of simulation experiments: test functions and datasets. URL: <http://www.sfu.ca/~ssurjano>.
- Wackers, J., Pellegrini, R., Serani, A., Visonneau, M., Diez, M., 2023. Efficient initialization for multi-fidelity surrogate-based optimization. Journal of Ocean Engineering and Marine Energy 9, 291–307.
- Wahba, G., 1990. Spline models for observational data. SIAM.
- Wendland, H., 2004. Scattered data approximation. volume 17. Cambridge university press.
- Wilson, A.G., 2014. Covariance kernels for fast automatic pattern discovery and extrapolation with Gaussian processes. Ph.D. thesis. University of Cambridge.
- Wilson, A.G., Gilboa, E., Cunningham, J.P., Nehorai, A., 2014. Fast kernel learning for multidimensional pattern extrapolation, in: Ghahramani, Z., Welling, M., Cortes, C., Lawrence, N.D., Weinberger, K.Q. (Eds.), Advances in Neural Information Processing Systems, Curran Associates, Inc.. pp. 3626–3634. URL: <https://proceedings.neurips.cc/paper/2014/hash/77369e37b2aa1404f416275183ab055f-Abstract.html>.
- Wilson, A.G., Nickisch, H., 2015. Kernel interpolation for scalable structured Gaussian processes (KISS-GP), in: Bach, F.R., Blei, D.M. (Eds.), Proceedings of the 32nd International Conference on Machine Learning, ICML 2015, Lille, France, 6-11 July 2015, JMLR.org. pp. 1775–1784. URL: <http://proceedings.mlr.press/v37/wilson15.html>.
- Wu, A., Aoi, M.C., Pillow, J.W., 2017. Exploiting gradients and Hessians in Bayesian optimization and Bayesian quadrature. ArXiv preprint abs/1704.00060. URL: <https://arxiv.org/abs/1704.00060>.
- Xiong, S., Qian, P.Z.G., Wu, C.F.J., 2013. Sequential design and analysis of high-accuracy and low-accuracy computer codes. Technometrics 55, 37–46.
- Zeng, X., Kritzer, P., Hickernell, F.J., 2009. Spline methods using integration lattices and digital nets. Constructive Approximation 30, 529–555.
- Zeng, X., Leung, K.T., Hickernell, F.J., 2006. Error analysis of splines for periodic problems using lattice designs. Springer.

Appendix A. Optimal Multitask Bayesian Cubature Weights

We are interested in finding some optimal weights $\omega \in \mathbb{R}^L$ which minimize the mean squared error (MSE)

$$\text{MSE}(\omega) = \mathbb{E}[(\omega^\top \boldsymbol{\mu} - \chi^\top \widehat{\boldsymbol{\mu}})^2 | \mathbf{y}] = \omega^\top \boldsymbol{\Sigma} \omega + (\omega^\top \widehat{\boldsymbol{\mu}} - \chi^\top \widehat{\boldsymbol{\mu}})^2. \quad (\text{A.1})$$

In the last equation above, the first term is the variance and the last term is squared bias.

Theorem Appendix A.1. $\omega = (\chi^\top \widehat{\boldsymbol{\mu}}) (\boldsymbol{\Sigma} + \widehat{\boldsymbol{\mu}} \widehat{\boldsymbol{\mu}}^\top)^{-1} \widehat{\boldsymbol{\mu}}$ attains the minimum MSE of $(\chi^\top \widehat{\boldsymbol{\mu}})^2 (1 - \widehat{\boldsymbol{\mu}}^\top (\boldsymbol{\Sigma} + \widehat{\boldsymbol{\mu}} \widehat{\boldsymbol{\mu}}^\top)^{-1} \widehat{\boldsymbol{\mu}})$ in (A.1).

Notice that regardless of χ , there is always a minimizer of $\text{MSE}(\omega)$ which is proportional to $(\boldsymbol{\Sigma} + \widehat{\boldsymbol{\mu}} \widehat{\boldsymbol{\mu}}^\top)^{-1} \widehat{\boldsymbol{\mu}}$.